Research Square

Preprints are preliminary reports that have not undergone peer review.
They should not be considered conclusive, used to inform clinical practice,
or referenced by the media as validated information.

Mass spectrometric profiling of plasma and erythrocyte glycerophospholipids and oxylipins in patients hospitalized with coronavirus disease 2019

Alaa Khedr
akhedr@kau.edu.sa
King Abdulaziz univer
Ahdab N. Khayyat
King Abdulaziz univer
Ahmed K. Kammoun
King Abdulaziz univer

Research Article

Keywords: COVID-19, lipidomics, erythrocytes, plasma, LC–MS/MS, ion-trap mass spectrometry, glycerophospholipids, oxylipins, applied analytical chemistry

Posted Date: November 3rd, 2026

DOI: https://doi.org/10.21203/rs.3.rs-11261109/v1

License: This work is licensed under a Creative Commons Attribution 4.0 International License. Read Full License

Additional Declarations: No competing interests reported.

Abstract

Coronavirus disease 2019 (COVID-19) is associated with systemic inflammation, oxidative stress, and altered lipid metabolism; however, paired characterization of plasma and erythrocyte lipid profiles remains limited. This exploratory case–control study evaluated an LC–linear ion-trap tandem mass spectrometry (LC–IT-MS/MS) workflow for profiling selected glycerophospholipids and oxidized fatty-acid mediators in paired plasma and erythrocyte samples from 30 hospitalized patients with moderate-to-severe COVID-19 and 30 healthy controls. Samples were subjected to nitrogen-protected biphasic chloroform–methanol extraction, and lipid species were characterized using chromatographic retention behavior, multistage fragmentation, and spectral-library comparison. Quantification was performed using class-representative calibration and class-matched internal standards, while group differences were evaluated using univariate analysis, effect-size estimation, false-discovery-rate adjustment, and exploratory principal component analysis. The method showed acceptable analytical performance, with linearity over 1–100 ng/mL (r^2 = 0.9951–0.9992), limits of quantification of 0.70–1.00 ng/mL, intra-day precision of 3.8–12.5%, and recoveries of 86.4–108.7%. COVID-19 was associated with compartment-specific lipid alterations, including decreased plasma lysophosphatidylcholines and plasmenyl-phosphatidylethanolamines; LPC 20:5 and LPC 20:3 decreased by approximately fourfold, while the combined abundance of six plasmenyl-phosphatidylethanolamine species decreased by 52.7%. In erythrocytes, PE 18:1/22:6 increased 1.5-fold (126.2 versus 82.5 μg/mL), whereas total lysophosphatidylethanolamines and phosphatidylinositols decreased 4.3-fold and 2.5-fold, respectively. Erythrocyte 9-HpOTrE, 5-HETE, and 13-HOTrE increased by 3.9, 3.6, and 2.0-fold, respectively, and exploratory principal component analysis showed separation between COVID-19 and control samples. Paired plasma–erythrocyte LC–IT-MS/MS profiling therefore identified group-associated, compartment-specific changes in glycerophospholipids and oxidized lipid mediators consistent with altered membrane-lipid remodeling and oxidative lipid metabolism in hospitalized COVID-19 patients. These associations require confirmation by untargeted quantitative LC–MS/MS using authentic standards and validation in independent, clinically characterized cohorts before considering biomarker, stratification, or monitoring applications.

1 Introduction

Coronavirus disease 2019 (COVID-19), caused by severe acute respiratory syndrome coronavirus 2 (SARS-CoV-2), ranges from uncomplicated respiratory illness to severe pneumonia, acute respiratory distress syndrome, multisystem involvement, and death [1, 2]. Beyond its respiratory manifestations, COVID-19 is associated with systemic inflammation, oxidative stress, endothelial disturbance, and metabolic alterations that may affect circulating and cellular lipid composition [3, 4]. Lipids contribute to membrane architecture, energy metabolism, inflammatory signaling, lipoprotein function, and host responses to viral infection. Consequently, altered lipid metabolism has been repeatedly observed in COVID-19 and may reflect both the systemic inflammatory state and changes in cell-membrane lipid remodeling [5–8].

Lipidomics is the systematic measurement and characterization of lipid molecular species in biological samples. In the present study, the analysis focused on selected glycerophospholipids (GPLs), including phosphatidylcholines (PCs), phosphatidylethanolamines (PEs), phosphatidylinositols (PIs), lysophosphatidylcholines (LPCs), lysophosphatidylethanolamines (LPEs), and ether-linked phospholipids. The study also evaluated selected oxidized lipid mediators (oxylipins), which are oxygenated fatty-acid derivatives that may reflect altered lipid oxidation and inflammatory lipid metabolism [9–11]. Plasmalogens, a subgroup of ether phospholipids containing a vinyl-ether bond, are of particular analytical and biological interest because they can undergo preferential oxidative modification and are involved in membrane lipid homeostasis [12–14].

Most clinical lipidomics studies in COVID-19 have focused on plasma or serum. Plasma reflects the circulating lipid environment, including lipoprotein-associated and soluble lipid species influenced by systemic inflammation, metabolism, diet, medication exposure, and acute illness. In contrast, erythrocytes provide a cell-associated membrane compartment with a distinct phospholipid composition and sustained exposure to the circulating environment over the cell's lifespan. Erythrocyte lipid composition may therefore capture membrane-associated lipid remodeling that is not fully represented by plasma measurements alone. Previous work has demonstrated altered erythrocyte lipid-related metabolites, including oxysterols and acylcarnitines, in patients with COVID-19, supporting the value of erythrocytes as a complementary matrix for investigating infection-associated metabolic changes [15–17]. Combined analysis of plasma and erythrocytes may thus provide a broader view of compartment-associated lipid alterations than either matrix alone.

Liquid chromatography coupled with tandem mass spectrometry (LC–MS/MS) is widely used for lipid profiling because chromatographic separation can reduce matrix complexity and tandem mass spectrometry provides structural information through characteristic fragmentation behavior [15, 18, 19]. In particular, LC coupled with linear ion-trap multistage mass spectrometry (LC–ion-trap MS^n) can characterize lipid classes and selected molecular species using retention behavior, precursor-ion detection, and diagnostic fragmentation patterns [15, 19, 20]. However, analytical challenges remain, including matrix effects, differential ionization among lipid classes, incomplete availability of authentic standards, co-elution of isomeric species, and the need for reproducible extraction and quality-control procedures in complex matrices such as plasma and erythrocyte homogenates [17, 18, 21, 22]. These considerations are particularly relevant when applying class-representative calibration approaches and when interpreting species-level measurements as semi-quantitative estimates.

Accordingly, we applied a paired plasma–erythrocyte LC–ion-trap MS/MS workflow to characterize group-associated differences in selected glycerophospholipids and oxidized lipid mediators in hospitalized COVID-19 patients and healthy controls. The workflow incorporated nitrogen-protected lipid extraction, chromatographic separation, positive- and negative-ion acquisition where appropriate, class-matched internal standards, and multistage fragmentation supported by spectral-library comparison. The primary aim was to evaluate the applicability of this analytical approach for paired plasma and erythrocyte lipid profiling. The clinical comparison was exploratory and intended to identify lipid features that may warrant targeted quantitative confirmation in independent, clinically characterized cohorts.

2 Materials and methodology

2.1 Materials

Reference materials and internal standards were purchased from Avanti Polar Lipids (Alabaster, AL, USA). Supplier-reported purity was ≥ 99% for each material, where specified. Class-representative calibrants were LPC 19:0, PC 17:0/17:0, PE 17:0/17:0, arachidic acid (C20:0), and PI 16:0/18:1. Internal standards were LPC 17:0, PC 19:0/19:0, PE 15:0/15:0, arachidonic acid-d11, and PI 16:0-d31/18:1. Unless an authentic standard was available, reported concentrations for individual endogenous molecular species were estimated using the calibration response of the corresponding class-representative standard and should be interpreted as quantitative.

2.2 Instrument

Qualitative and quantitative analyses were performed using a Thermo Scientific LTQ-XL linear ion trap mass spectrometer, coupled with an Accela autosampler and Accela pump (San Jose, CA, USA). The electrospray ionization (ESI) compartment was used as the ion source. The system was operated with Xcalibur® software (version 2.07 SP1) from Thermo Fisher Scientific Inc. The spray voltage was 5.0 kV; the sheath gas flow rate was 40 mL/min; the auxiliary gas was 5 mL/min; the capillary voltage was 60 v; the capillary temperature was 345°C. The collision energy was 35 V. The column was an Eclipse Plus C18 (3.5 µm, 4.6 x 150 mm; Agilent, Palo Alto, USA), with a column oven at 40 ± 2°C and a tray temperature at 25°C. The mobile system was composed of (A) water: methanol: ammonium hydroxide solution 25% (75: 25: 0.4, v/v), (B) methanol: chloroform: ammonium hydroxide solution 25% (96: 4: 0.4, v/v), and (C) methanol: chloroform: ammonium hydroxide solution 25% (75: 25: 0.4, v/v). The flow rate was 400 µL/min. The LC gradient was programmed as follows: 0–2 min; 65%A: 35%B, gradient changed to 35%A: 65%B at 9 min, decreased to 15%A: 85%B at 30 min, to 5%A: 95%B at 40, to 1%A: 99%B at 49–70 min, switched to 100%C at 71 min, and followed by equilibration for 10 min at 65%A with 35%B, applying a dependent auto-MS fragmentation mode. The IT-MS detector was set to monitor ions in both positive and negative scan modes over a mass range of 100–1200 m/z. The LC-MS^n raw file was further investigated using Thermo Xcalibur 4.5.474.0 (1/14/2022) and FreeStyle™ 1.8 SP2 (Modern Data Visualization Software, Version 1.8.63.0, Build Date: July 30, 2021, Copyright © 2021 Thermo Fisher Scientific Inc.). The NIST2020 Mass Spectral Search Program was used to confirm the retrieved mass spectra of the targeted lipids. (Version 2.4, built on March 25, 2020). The NIST database was enriched by the online MassBank of North America (MoNA) and metadata-centric (https://mona.fiehnlab.ucdavis.edu).

2.3 Solutions and calibration levels

A mixture of chloroform and methanol (2:1, v/v) was used as the solvent matrix to prepare standard stock solutions and all other dilutions. One liter of this solvent was sparged with nitrogen gas (99.99%) for 5 minutes to remove dissolved oxygen. The internal standard (IS) solution was prepared in the same solvent to contain 50 ng/µL of each IS. A standard solution mixture of lipids used as calibrant was prepared to contain 2.0 to 200.0 ng/µL each of LPC 19:0, PC (17:0/17:0), PE (17:0/17:0), C20:0, and PI (16:0/18:1). The internal standard solution mixture was prepared to contain 50 ng/µL of each, LPC 17:0, PC (19:0/19:0), PE (15:0/15:0), arachidonic acid-d11, and PI (16:0-d31/18:1).

Eight calibration solution levels were prepared by mixing 25 µL of the internal standard solution mixture (50 ng/µL) with 100 µL of control plasma spiked with 25 µL of the calibrant mixture. The spiked control plasma samples were extracted and reconstituted in 100 µL of methanol.

The final calibrant concentration ranged from 1 to 100 ng/µL, with each IS at a constant concentration of 25 ng/µL. A volume of 5 µL was injected for LC-MS analysis. Calibration was based on the analyte-to-internal-standard peak-area ratio versus nominal concentration.

A linear calibration curve was plotted as the relative MS peak area of each calibrant to the corresponding internal standard versus the calibrant concentration. The MS area ratio of the calibrants to the internal standards was assigned as the following pairs; LPC 19:0 (+ *m/z* 538.4)/LPC 17:0 (+ *m/z* 510.3), PC (17:0/17:0) (+ *m/z* 762.6)/ PC (19:0/19:0) (+ *m/z* 818.6), PE (17:0/17:0) (+ *m/z* 720.5)/ PE (15:0/15:0) (+ *m/z* 664.5), C20:0 (-*m/z* 311.2)/ C20:4_d11 (-*m/z* 314.3), PI (16:0/18:1) (-*m/z* 835.5)/ PI (16:0-d31/18:1) (-*m/z* 883.8). Plasma and erythrocyte matrices were evaluated separately for ion suppression by spiking, extracting, and analyzing each matrix independently.

2.4 Study design and participants

Patients with general symptoms of COVID-19 infection, such as fever, chest pain with respiratory complaints, and general fatigue, are immediately subjected to the polymerase chain reaction (PCR) test. The nasopharyngeal swab sample is collected from the COVID-19 candidate and subjected to PCR testing, given its high specificity and sensitivity [23]. PCR is a method used to detect and identify the DNA or RNA of a pathogen or atypical cell within a sample. This technique uses primers that bind to specific segments of genetic material and amplify them to levels detectable by the assay. A PCR test for COVID-19 targets explicitly the virus's RNA, which causes illness. Known for its speed, accuracy, and sensitivity, this test is the gold standard for diagnosing COVID-19. This study included only hospitalized patients clinically diagnosed with moderate to severe COVID-19 infection, in accordance with international guidelines for COVID-19 severity [24]. Patients diagnosed as asymptomatic were excluded. COVID-19 severity was classified according to standard clinical criteria [25]. Mild cases presented with fever, cough, and general symptoms without respiratory compromise or hypoxemia. Moderate cases exhibited dyspnea, tachypnea, and oxygen saturation ≤ 93% on room air, often accompanied by laboratory evidence of systemic inflammation such as lymphocytopenia or elevated C-reactive protein. Severe cases showed marked respiratory distress with persistent hypoxemia despite oxygen supplementation, PaO_2/FiO_2 <300 mmHg, and frequently elevated D-dimer or cardiac biomarkers, indicating progression toward acute respiratory failure and systemic involvement. The plasma and erythrocyte samples collected and analyzed from each participant were paired; however, the analyses did not account for within-person pairing.

The study exclusion criteria included pregnant women, volunteers receiving any hypolipidemic drugs or statins, diabetic patients, cases who received streptokinase injections, and acute cases on mechanical ventilation. This study included 30 healthy volunteers and 30 COVID-19 patients, with equal male and female representation. The volunteers were aged 40–75 and admitted to the hospital under medical supervision. Patients read, understood, and signed the informed consent form, which the hospital archived securely. Healthy volunteers were carefully selected and had recent medical investigations within 7 days at King Abdulaziz University Hospital in Jeddah, Saudi Arabia.

2.5 Blood sample collection

A 5 mL blood sample volume was collected from the antecubital vein into sodium-EDTA tubes, swirled, and immediately sent to the analysis lab. The blood samples were centrifuged at 3000 rpm for 15 min. The supernatant plasma was aspirated with a Pasteur pipette, transferred to a 7-mL brown-glass vial, and kept at -80°C until analysis.

The red residue was separated, mixed with 5 mL saline (0.9% sodium chloride in water, w/v) by gentle swirling, and centrifuged at 2800 rpm for 15 min. The upper aqueous layer was aspirated and discarded. The remaining erythrocytes were vortexed for 1 min and then placed in a sonication bath for 15 min to homogenize the ruptured erythrocytes. The homogenate erythrocyte samples were either extracted immediately or kept at -80°C until analysis. The plasma and erythrocyte samples were bubbled with nitrogen gas for 30 seconds before storage or analysis.

2.6 Sample preparation for the analysis

A volume of 100 µL of plasma or erythrocyte homogenate was transferred to a screw-capped 15-mL glass test tube, mixed with 6 mL of the extraction solvent (chloroform: methanol, 2: 1, v/v), 25 µL of the IS solution mixture, and left under a gentle stream of nitrogen gas for 30 sec before capping. Vortexed the mixture for 2 minutes, sonicated for 15 minutes, vortexed for 30 seconds, and centrifuged at 5000 rpm for 15 minutes. The organic layer was separated by decantation into a 25-mL syringe fitted with a 0.22 µm PTFE filtration membrane, filtered into a 15-mL glass test tube, and dried with nitrogen gas over a water bath at 40°C. The remaining residue was quantitatively transferred to a 1 mL total recovery vial using 200 µL of the same extraction solvent, and the vial was gently bubbled with nitrogen gas to dryness. The residue was reconstituted in 50 µL chloroform: methanol (2:1, v/v), capped under nitrogen, vortexed, and 5 µL was injected for LC-IT-MS analysis. Plasma samples were analyzed in positive MS mode, while erythrocyte extract samples were analyzed in both positive and negative MS modes. Four plasma quality-control (QC) samples were prepared at calibrant-mixture concentrations of 5, 25, 50, and 100 ng/mL. The QC samples were stored with the study samples at − 80°C and analyzed during the same week as the study samples.

Each analyte was quantified by extracting its corresponding precursor-ion chromatogram from the LC–IT–MS data within the specified retention-time window and integrating the peak area. The analyte concentration was then determined from the linear calibration equation, using the analyte-to-assigned-internal-standard peak-area ratio as the y-value.

That species without authentic standards are semi-quantitative estimates based on class-representative calibration.

2.7 Characterization of lipids

The extracted samples were subjected to IT-MSn to identify minor and major compounds derived from biogenic lipids. After lipid characterization, the mean IT-MS^2 spectra of the targeted lipids were retrieved using a collision energy of 35 V and re-analyzed by assigning the peak of interest to its corresponding retention time. The IT-MS^2 spectra of the detected precursor ions were investigated and confirmed by the NIST 2020 database. The NIST database was updated to a release of 2022 using a retrievable NIST-format online database of the Mass Bank of North America (MoNA) at https://mona.fiehnlab.ucdavis.edu.

2.8 Statistical analysis

The LC-MS data were quantitatively processed using Thermo Scientific Xcalibur, version 4.6.67.17. The output quantitative report and calibration data were saved as Microsoft Excel files. All univariate statistical parameters, including mean concentration, standard deviation, variance, and t-test, were calculated and evaluated using Microsoft Excel. Samples with results outside the valid determination range were re-prepared at a higher or lower final expected concentration to fall within the valid calibration range. The quantitative results from healthy and COVID-19 patients were statistically evaluated using principal component analysis (PCA) to determine the score profile in the Multivariate Statistical Package (MVSP, version 3.22, Kovach Computing Services, Pentraeth, Isle of Anglesey, UK, 2013).

We calculated a statistical refinement directly from the group means, standard deviations, and sample sizes shown in Tables 2–4. It includes effect sizes, reconstructed Welch t-test p-values [26], Benjamini–Hochberg false-discovery-rate (FDR) [27] adjustment, an interpretive summary, and a supplementary figure. To provide an effect-size and multiple-testing perspective, a secondary analysis was conducted using the calculated group means, standard deviations, and sample sizes (n = 30 per group) for the lipid species listed in Tables 2–4. For each lipid, the COVID-19/control fold change and log2 fold change were calculated. Standardized mean differences were estimated as Hedges' g [28] using the pooled standard deviation and a small-sample correction. Two-sided Welch t-test p-values were reconstructed from summary statistics and adjusted separately within each table/panel using the Benjamini–Hochberg false-discovery-rate (FDR) procedure [27]. These results are intended as a supplementary robustness analysis.

3 Results and discussion

To thoroughly characterize lipid species, multiple fragmentation steps (MS^n) were applied [29], including extraction, separation, identification, and quantification. This integrated workflow provides a detailed view of lipid profiles and their potential relevance to neurological and cognitive disturbances in diseases such as COVID-19, as each technique provides complementary information.

3.1 Method optimization and validation

Ion trap mass spectrometry (IT-MS) was preferred for quantitative phospholipid (PL) analysis over other MS techniques. As absolute quantification of PLs remains challenging with any single analytical method, untargeted IT-MS operated in scan mode was used to confirm the presence of the target analyte at its corresponding retention time. The LC-MS method was optimized to achieve optimal lipid separation, especially for co-eluting lipids at 40–70 min. The developed method showed fewer peak overlaps, thereby minimizing ionization suppression. The method also provided optimal detection sensitivity. In addition, a multi-step fragmentation strategy was used to assign each fatty acid to its precursor ion [15]. Moreover, the lipids of similar precursor ions, specifically isomers or etherial lipids, negative or positive, were discriminated and identified [19].

Factors influencing data quality were acknowledged as potential variables, as highlighted in the Myers Review [18]. To preserve lipid chemical integrity, samples were kept under nitrogen gas throughout the extraction process. The MS-identified lipids were confirmed with repeated analyses using fragmentation voltages of 25, 35, and 45V and the NIST2020 database. The separated lipid entities were also screened using an ultra-zoom ESI-MS scan and zoomed-fragmentation mode to more accurately identify dysregulated lipids. The targeted analytes, including abnormal lipids, were then considered for quantitative analysis.

A previously published LC-IT-MS method was modified and optimized, and the technique was applied [15]. Lipid levels in healthy and COVID-19 patients were compared and statistically analyzed for significant differences. All samples were analyzed quantitatively by applying a collision energy of 35 volts. Peak picking was completed after confirmation with the enriched NIST2020 database. The dysregulated lipid composition in the plasma and erythrocytes of COVID-19 patients was investigated versus that of healthy control subjects.

A modified Bligh and Dyer [21] extraction method was optimized and applied in this study to recover the highest possible lipid content from plasma and erythrocytes. Several extraction trials have been conducted to obtain an extract with the highest yield, purity, and low red pigmentation [17, 30]. The extraction protocol was optimized to maximize lipid recovery while ensuring extract purity and preserving the chemical integrity and stability of the target lipid species. All extraction procedures were carried out under nitrogen gas to prevent auto-oxidation of the biomolecules. This step helped avoid misleading results. Samples with extra-red pigmentation were re-extracted at a slower centrifugation rate of 2500 rpm for 15 minutes. These samples were obtained from volunteers with severe COVID-19. The study profiled lipid species in plasma and erythrocytes, including glycerophospholipids, plasmenyl-glycerophospholipids, and oxidized lipid mediators (oxylipins). Dysregulated lipid species were subsequently examined for their association with the clinical manifestations of COVID-19.

The LC–IT–MS/MS validation data demonstrate that the method provides adequate analytical performance for the class-based, quantitative profiling of glycerophospholipids and selected oxidized fatty-acid mediators in human plasma and erythrocyte homogenates. Table 1 summarizes the method validation data.

Table 1
Validation results of investigated analytes

Analyte class/calibrant	Internal standard	Linearity range, ng/mL	R^2	LOD, ng/mL	LOQ, ng/mL	Intra-day precision (%RSD)	Inter-day precision (%RSD)	Accuracy /recovery (%)	Matrix effect: plasma (%)	Matrix effect: erythrocytes (%)
LPC; LPC 19:0	LPC 17:0	1–100	0.9992	0.20	0.70	3.8–8.6	5.2–10.4	92.1–106.8	93.5–105.6	89.8–108.4
PC; PC 17:0/17:0	PC 19:0/19:0	1–100	0.9986	0.30	1.00	4.5–10.2	6.3–12.7	89.4–104.5	90.2–106.7	87.1–110.9
PE; PE 17:0/17:0	PE 15:0/15:0	1–100	0.9978	0.35	1.00	5.1–11.3	7.0–14.2	86.4–102.8	88.1–104.9	84.7–109.6
Fatty acid/oxylipin surrogate; C20:0	Arachidonic acid-d11	1–100	0.9951	0.45	1.00	4.8–12.5	6.9–14.8	88.7–108.7	91.8–109.3	88.5–112.6
PI; PI 16:0/18:1	PI 16:0-d31/18:1	1–100	0.9967	0.40	1.00	5.6–11.8	7.4–13.9	87.6–105.3	89.6–106.1	86.2–111.3

Table 2
Plasma concentrations of dysregulated GPLs in healthy subjects and COVID-19-infected patients. The *p*-values were calculated at probability ± 0.05, with n = 30

t_R, min	Name	Ion, *+m/z*	HP, µg/mL ± SD		CP, µg/mL ± SD		*p*-value	*
24.23	LPC 14:0	468.4	1.18	± 0.54	0.59	± 0.44	< 0.001	↓
24.96	LPC 15:0	482.4	0.73	± 0.37	0.31	± 0.25	< 0.001	↓
34.61	LPC O-16:0	482.4	3.33	± 2.98	0.70	± 0.48	< 0.001	↓
24.76	LPC 16:0	496.4	91.55	± 21.92	50.88	± 20.21	< 0.001	↓
36.33	LPC O-18:1	508.4	0.79	± 0.35	0.33	± 0.18	< 0.001	↓
39.44	LPC P18:0	508.4	0.65	± 0.28	0.17	± 0.17	< 0.001	↓
25.30	LPC 18:3	518.3	0.45	± 0.26	0.19	± 0.18	< 0.001	↓
28.12	LPC 18:2	520.4	49.55	± 22.80	16.67	± 8.18	< 0.001	↓
31.91	LPC 18:1	522.4	28.56	± 10.67	14.43	± 7.28	< 0.001	↓
36.22	LPC 18:0	524.4	27.43	± 8.29	15.39	± 6.89	< 0.001	↓
25.33	LPC 20:5	542.4	1.04	± 0.80	0.25	± 0.19	< 0.001	↓
28.12	LPC 20:4	544.4	20.09	± 8.33	10.92	± 5.08	< 0.001	↓
30.81	LPC 20:3	546.4	8.52	± 6.13	2.24	± 1.51	< 0.001	↓
38.16	LPC 20:1	550.4	0.45	± 0.25	0.20	± 0.15	< 0.001	↓
28.56	LPC 22:6	568.4	3.83	± 2.35	1.89	± 1.13	< 0.001	↓
56.71	PC (15:0/20:4)	768.5	17.20	± 6.77	10.49	± 6.35	< 0.001	↓
54.08	PC (18:2/18:2)	782.5	20.12	± 10.92	9.18	± 4.59	< 0.001	↓
55.61	PC (16:0/20:3)	784.5	102.49	± 30.31	78.79	± 30.53	< 0.001	↓
56.32	PC (18:0/18:2)	786.5	153.12	± 85.17	113.34	± 46.02	< 0.001	↓
56.77	PC (18:1/20:2)	812.5	52.41	± 30.14	34.53	± 11.27	< 0.001	↓
55.88	PC (18:0/22:6)	834.6	14.55	± 5.94	9.43	± 4.50	< 0.001	↓
55.60	PC (16:1/20:5)	778.5	3.51	± 1.58	6.74	± 4.50	< 0.001	↑
55.22	PC (16:0/16:1)	732.5	7.77	± 3.32	13.68	± 7.28	< 0.001	↑
	PEs decreased							
39.70	PE (P16:0/20:4)	724.5	5.63	± 2.26	2.88	± 1.19	< 0.001	↓
41.90	PE (15:0/20:4)	726.5	2.70	± 1.33	1.38	± 0.78	< 0.001	↓
43.57	PE (P18:0/18:1)	730.5	1.14	± 0.43	0.57	± 0.35	< 0.001	↓
39.68	PE (18:1/18:2)	742.5	3.51	± 1.97	1.91	± 1.10	< 0.001	↓
39.29	PE (P16:0/22:6)	748.5	2.47	± 0.88	1.33	± 0.50	< 0.001	↓
42.52	PE (O-16:1/22:6)	748.5	3.06	± 1.08	1.53	± 0.57	< 0.001	↓
43.18	PE (P18:0/20:5)	750.5	6.35	± 3.30	3.06	± 1.88	< 0.001	↓
40.51	PE (P16:0/22:5)	750.5	2.37	± 1.82	0.81	± 0.38	< 0.001	↓
42.71	PE (P18:0/20:4)	752.5	8.79	± 3.54	4.00	± 2.26	< 0.001	↓
41.80	PE (22:6/17:1)	776.3	2.51	± 1.13	1.46	± 0.58	< 0.001	↓

* Statistical significance, ↑ a significant increase, ↓ a significant decrease. HP: Healthy plasma samples; CP: COVID-19 plasma samples; LPEs: Lysophosphatidylethanolamines; LPCs: Lysophosphatidylcholines; phosphatidylethanolamine; PE, phosphatidylcholine; PC, SD: Standard deviation.

t_R, min	Name	Ion, *+m/z*	HP, µg/mL ± SD		CP, µg/mL ± SD		*p*-value	*
	PEs increased							
40.24	PE (16:0/18:1)	718.5	2.84	± 1.76	4.71	± 2.05	< 0.001	↑
39.06	PE (16:0/20:4)	740.5	2.50	± 1.02	6.92	± 6.39	< 0.001	↑
38.94	PE (16:0/22:6)	764.5	2.40	± 1.57	4.53	± 1.65	< 0.001	↑
39.22	PE (18:0/20:5)	766.5	0.67	± 0.46	1.46	± 0.79	< 0.001	↑
39.30	PE (18:1/20:4)	766.5	1.30	± 0.75	2.71	± 1.44	< 0.001	↑
40.86	PE (16:0/22:4)	768.3	11.39	± 7.61	16.88	± 5.09	0.011	↑
38.21	PE (18:3/22:6)	786.5	0.67	± 0.47	1.30	± 0.52	< 0.001	↑
42.25	PE (18:1/22:5)	792.5	3.31	± 2.26	5.07	± 1.75	0.010	↑

* Statistical significance, ↑ a significant increase, ↓ a significant decrease. HP: Healthy plasma samples; CP: COVID-19 plasma samples; LPEs: Lysophosphatidylethanolamines; LPCs: Lysophosphatidylcholines; phosphatidylethanolamine; PE, phosphatidylcholine; PC, SD: Standard deviation.

The squared regression coefficient was close to unity, and the response factor was close to 0.04. The ESI source was maintained and tuned daily at + *m/z* 524.33 to minimize ionization suppression caused by contamination of the ion source. Samples that showed analyte concentrations outside the calibration range were diluted or concentrated using nitrogen gas to obtain an ESI-MS response within the valid range.

All representative lipid classes showed acceptable linearity over 1–100 ng/mL, with r2 values of 0.9951–0.9992, while the low LODs (0.20–0.45 ng/mL) and LOQs (0.70–1.00 ng/mL) confirmed sufficient sensitivity for detecting low-abundance lipid signals. Intra- and inter-day precision remained within 3.8–12.5% and 5.2–14.8% RSD, respectively, and extraction recoveries of 86.4–108.7% indicated reproducible sample preparation across chemically diverse lipid classes. Matrix effects were modest in both plasma and erythrocyte homogenates, particularly after normalization with class-matched internal standards, supporting the robustness of the workflow in these complex biological matrices. The novelty of this approach lies in its integrated validation and application to paired plasma and erythrocyte samples, enabling simultaneous assessment of circulating lipids and erythrocyte membrane-associated lipid remodeling. Unlike many COVID-19 lipidomic studies focused exclusively on plasma and high-resolution discovery platforms, this work uses accessible LC–ion-trap multistage MS with class-specific internal standards, confirmation by diagnostic fragmentation, and a nitrogen-protected extraction procedure to support reproducible detection of glycerophospholipids, plasmalogens, lysophospholipids, phosphatidylinositols, and oxylipins.

3.2 Group-associated differences in plasma and erythrocyte lipid profiles

Special attention was drawn to the relatively abundant lipids that exhibited significant up- or down-regulation. Additionally, the biological functions of each lipid class were correlated with the clinical symptoms. The observed group differences are consistent with altered plasma and erythrocyte lipid composition in hospitalized COVID-19. Because this study did not measure viral membrane interactions or membrane function, the data do not establish a direct viral mechanism.

Lipid dysregulation alters the optimal conditions required for viral replication, leading to a specific composition [7]. The LC-MS results revealed significant dysregulation of glycerophospholipids (GPLs) in the plasma and erythrocytes of COVID-19 patients compared to healthy volunteers (Table 2–3).

Table 3
The measured concentration of the dysregulated GPLs in the erythrocytes of healthy volunteers and COVID-19 patients. The *p*-values were calculated at probability ± 0.05, with n = 30

t_R, min	Name	Ion, *+m/z*	HR, µg/mL ± SD		CR, µg/mL ± SD		*p*-value	*
24.96	LPC 15:0	482.4	0.13	± 0.15	0.51	± 0.17	< 0.001	↑
19.01	LPE 18:0	482.4	0.10	± 0.05	0.20	± 0.26	0.041	↑
15.09	LPE 22:6	526.4	0.17	± 0.10	3.72	± 1.88	< 0.001	↑
17.21	LPE 16:0	454.4	3.79	± 1.88	0.57	± 0.99	< 0.001	↓
17.91	LPE 17:0	468.3	1.02	± 0.51	0.24	± 0.33	< 0.001	↓
15.56	LPE 18:1	480.4	3.24	± 1.28	0.41	± 0.73	< 0.001	↓
14.24	LPE 18:3	476.4	2.71	± 1.59	0.24	± 0.37	< 0.001	↓
19.10	LPE 20:4	502.2	3.08	± 1.61	1.76	± 1.49	< 0.001	↓
14.41	LPE 20:5	500.4	0.82	± 0.74	0.20	± 0.17	< 0.001	↓
54.17	PC (16:1/16:1)	730.5	1.02	± 0.75	8.46	± 5.22	< 0.001	↑
59.55	PC (18:0/18:1)	788.5	24.83	± 7.36	33.61	± 9.38	< 0.001	↑
55.22	PC (20:4/20:5)	828.5	4.88	± 0.93	10.25	± 3.56	< 0.001	↑
55.50	PC (15:0/20:5)	766.5	1.90	± 1.22	0.29	± 0.21	< 0.001	↓
55.69	PC (16:0/18:3)	756.5	3.49	± 1.37	2.23	± 1.26	< 0.001	↓
55.09	PC (16:0/18:4)	754.5	2.38	± 1.47	1.20	± 0.38	< 0.001	↓
55.61	PC (16:0/20:3)	784.5	29.62	± 9.21	11.47	± 7.13	< 0.001	↓
55.00	PC (16:0/20:5)	780.5	4.99	± 3.37	2.26	± 2.76	< 0.001	↓
56.20	PC (16:0/22:4)	810.6	3.91	± 0.67	2.19	± 1.18	< 0.001	↓
55.81	PC (16:0/22:6)	806.6	14.23	± 8.62	6.59	± 4.61	< 0.001	↓
55.60	PC (16:1/20:5)	778.5	3.27	± 3.06	0.81	± 0.81	< 0.001	↓
55.04	PC (18:0/20:4)	810.6	11.78	± 6.59	7.76	± 3.77	0.010	↓
56.34	PC (18:0/20:5)	808.6	7.27	± 1.54	3.07	± 1.91	< 0.001	↓
55.39	PC (18:1/20:4)	808.6	5.36	± 2.42	2.64	± 0.96	< 0.001	↓
54.08	PC (18:2/18:2)	782.5	5.03	± 5.02	0.34	± 0.54	< 0.001	↓
55.88	PC (18:2/20:5)	804.5	4.60	± 1.55	2.68	± 1.84	< 0.001	↓
56.65	PC (18:2/22:4)	834.5	8.48	± 5.14	3.95	± 1.95	< 0.001	↓
	PEs increased							
40.24	PE (16:0/18:1)	718.5	21.75	± 5.72	30.64	± 6.66	< 0.001	↑
42.81	PE (18:0/18:1)	746.5	9.39	± 2.42	17.73	± 3.93	< 0.001	↑
43.68	PE (18:0/22:6)	792.5	2.52	± 1.43	3.78	± 2.00	0.011	↑
44.76	PE (18:1/20:0)	774.3	23.48	± 8.63	33.92	± 20.98	0.012	↑
42.58	PE (18:1/22:5)	792.5	3.94	± 1.53	9.32	± 4.57	< 0.001	↑
42.56	PE (18:1/22:6)	790.5	82.46	± 33.82	126.15	± 73.47	< 0.001	↑
38.21	PE (18:3/22:6)	786.5	0.78	± 0.37	1.84	± 0.71	< 0.001	↑

* Statistical significance, ↑ a significant increase, ↓ a significant decrease. HR: Healthy RBCs samples; CR: COVID-19 RBCs samples; LPEs: Lyso-phosphatidylethanolamines; LPCs: Lys-phosphatidylcholines; phosphatidylethanolamine; PE, phosphatidylcholine; PC, SD: Standard deviation.

t_R, min	Name	Ion, *+m/z*	HR, µg/mL ± SD		CR, µg/mL ± SD		*p*-value	*
48.00	PE (22:6/17:1)	776.3	14.21	± 4.09	38.33	± 24.97	< 0.001	↑
	PEs decreased							
40.50	PE (16:0/20:5)	738.5	1.07	± 1.10	0.43	± 0.47	0.010	↓
39.22	PE (18:0/20:5)	766.5	1.58	± 0.68	0.65	± 0.57	< 0.001	↓
44.11	PE (18:0/22:5)	794.5	4.89	± 2.25	2.09	± 0.97	< 0.001	↓
39.30	PE (18:1/20:4)	766.5	5.26	± 3.30	3.75	± 1.63	0.030	↓
40.00	PE (18:2/16:0)	716.5	5.33	± 4.65	1.60	± 2.63	< 0.001	↓
41.50	PE (22:4/18:0)	796.5	4.62	± 2.44	0.61	± 1.21	< 0.001	↓
44.89	PE (22:5/18:0)	794.5	18.02	± 22.49	3.00	± 1.28	< 0.001	↓
40.51	PE (P16:0/22:5)	750.5	0.99	± 0.83	0.28	± 0.25	< 0.001	↓
43.57	PE (P18:0/18:1)	730.5	4.10	± 1.55	1.51	± 1.14	< 0.001	↓

* Statistical significance, ↑ a significant increase, ↓ a significant decrease. HR: Healthy RBCs samples; CR: COVID-19 RBCs samples; LPEs: Lyso-phosphatidylethanolamines; LPCs: Lys-phosphatidylcholines; phosphatidylethanolamine; PE, phosphatidylcholine; PC, SD: Standard deviation.

Tables 1–3 showed the most dysregulated glycerophospholipids (GPLs) in the plasma and erythrocytes of COVID-19 patients compared to healthy volunteers. Considering that the sum of GPLs in the erythrocytes is not expressive, PE (16:0/18:1), PE (18:1/20:0), PE (22:6/17:1), PC (18:0/18:1), and PE (18:1/22:6) correspond to the highest concentrations of total dysregulated lipids and are significantly accumulated. The results showed significant increases or decreases in specific lipid levels in plasma and erythrocytes. Patients infected with COVID-19 showed a definite abnormal pattern in GPL levels, as shown in Tables 1–3. The findings indicated significant alterations in glycerophospholipid (GPL) levels in both plasma and erythrocytes, with specific lipids showing either increased or decreased levels. Notably, COVID-19 patients showed a distinct abnormal pattern of GPL levels, as shown in Tables 1–3. In COVID-19 patients, glycerophospholipids within erythrocytes exhibited notable accumulation of PE (18:1/22:6), resulting in a concentration of 126.2 µg/mL (a 1.5-fold increase, as indicated in Table 3).

In COVID-19 patients, six glycerophospholipid species containing arachidonic-acid acyl chains exhibited significant plasma differences. Specifically, PC (18:0/18:2) and PC (16:0/20:3) accounted for 38% of down-regulated GPLs, showing a 24.8% decrease, aligning with healthy volunteer levels. While PE (16:0/22:4) was markedly upregulated by 1.5-fold, the combined concentration of PC (15:0/20:4), PE (P18:0/20:4), PE (P16:0/20:4), and PE (15:0/20:4) considerably decreased by 20.3%. Concurrently, the combined plasma concentration of PE (16:0/20:4) and PE (18:1/20:4) increased by 90.4%.

Table 4
The measured concentration of the oxi-lipids and PIs in the erythrocytes of healthy volunteers and Covid-19 hospitalized cases. *p*-Values calculated at probability ± 0.05, n = 30

t_R, min	Name	Ion, *-m/z*	HR, µg/mL ± SD		CR, µg/mL ± SD		*p*-value	*
8.5	ALA, C18:3	277.2	1.77	± 1.84	3.08	± 1.87	0.010	↑
12.12	13-HOTrE	293.2	1.87	± 1.77	3.77	± 3.16	0.011	↑
11.01	9-HpOTrE	309.2	3.18	± 2.31	12.45	± 18.87	0.011	↑
8.79	5-HETE	319.2	0.37	± 0.36	1.35	± 1.86	0.010	↑
12.42	LPI 20:4	619.3	0.40	± 0.53	0.96	± 0.90	0.010	↑
12.05	LA, C18:2	279.2	22.76	± 32.93	4.49	± 8.41	0.011	↓
12.38	AA, C20:4	303.2	9.14	± 9.10	3.54	± 3.05	0.010	↓
12.51	C20:4-d11, IS	314.3	N/A	N/A	N/A	N/A	N/A	-
15.88	LPI 18:0	599.3	7.95	± 6.96	2.15	± 1.73	< 0.001	↓
34.47	PI (16:0/18:2)	833.5	2.23	± 2.05	0.62	± 0.93	< 0.001	↓
34.55	PI (16:0/20:4)	857.5	2.66	± 3.36	0.87	± 0.66	0.012	↓
35.93	PI (16:0/18:1)	835.5	5.79	± 5.49	3.22	± 2.07	0.030	↓
36.87	PI (18:0/18:2)	861.5	3.24	± 3.19	1.01	± 1.09	< 0.001	↓
36.89	PI (18:0/20:4)	885.5	17.99	± 13.87	7.69	± 5.34	< 0.001	↓
38.19	PI (18:1/18:0)	863.5	3.35	± 3.29	1.48	± 1.37	0.011	↓
37.74	PI (18:0/20:3)	887.5	1.61	± 1.08	1.00	± 0.60	0.020	↓
36.30	PI (16:0-d31-18:1)	883.8	N/A	N/A	N/A	N/A	N/A	-

* Statistical significance, ↑ a significant increase, ↓ a significant decrease. HR: Healthy RBCs samples; CR: COVID-19 RBCs samples; PI: phosphatidylinositol, LA: linoleic acid

Both PC (18:0/18:2) and LPC 18:2 accounted for 30.1% of the total dysregulated GPLs, with 35.8% downregulated. Additionally, LPC 20:5 and LPC 20:3 were downregulated approximately 4.0-fold. Several other lysophosphatidylcholines (LPCs), including LPC 14:0, LPC 15:0, LPC O-16:0, LPC 16:0, LPC O-18:1, and LPC P18:0, also showed significant plasma downregulation. The broad reduction in several plasma LPC species indicates altered lysophospholipid abundance in hospitalized COVID-19. The present data do not distinguish among altered production, reacylation, lipoprotein distribution, inflammatory metabolism, medication effects, diet, or pre-analytical influences. Beyond the specific changes observed in PC 18:0/18:2 and PC 16:0/20:3, the significant downregulation of additional phosphatidylcholine species indicates a broader remodeling. These alterations could affect membrane fluidity and lipid raft organization, both critical for viral entry and propagation. Furthermore, six plasmenyl-phosphatidylethanolamines (PE (P16:0/20:4), PE (P18:0/18:1), PE (P16:0/22:6), PE (P18:0/20:5), PE (P16:0/22:5), and PE (P18:0/20:4)) were reduced by approximately 52.7% in plasma.

In erythrocytes, COVID-19 patients displayed a significant accumulation of PE (18:1/22:6), reaching 126.2 µg/mL (1.5× higher than controls). Notably, LPC 15:0 was significantly increased in erythrocytes, contrasting with the general LPC decline observed in plasma. This result suggests compartment-specific lipid alterations and potential erythrocyte membrane remodeling, which could affect cell deformability and oxygen transport. Regulation of lysophosphatidylethanolamines (LPEs) in erythrocytes appears uneven, with elevations in LPE 18:0 and LPE 22:6 contrasting with reductions in other species. This pattern points to selective catabolic or synthetic pathways modulated by SARS-CoV-2 infection. The significant elevation of specific phosphatidylcholine species (PC (16:1/16:1), PC (18:0/18:1), and PC (20:4/20:5)) in erythrocytes might represent a compensatory mechanism to maintain membrane integrity or respond to oxidative stress. Conversely, decreased erythrocyte levels of PC (15:0/20:5) and PC (16:0/18:3) may correlate with dysregulated fatty acid composition, potentially affecting membrane fluidity and cell signaling.

It has been reported that dysregulation of PEs in mammalian cells is often associated with Alzheimer's and Parkinson's disease [31]. Plasmalogens play a crucial role as endogenous antioxidants, protecting other PLs, lipids, and lipoprotein particles from oxidative stress [13]. This antioxidant effect is attributed to preferential oxidation of the vinyl ether bond, thereby protecting the polyunsaturated fatty acids in the sn-2 position [12]. This illustration supports this study's evidence that COVID-19 infection leads to oxidative stress in cellular GPLs. Altered phospholipid and ether-lipid abundance may be relevant to membrane-lipid biology; however, this study did not assess membrane mechanical

properties or cognitive outcomes. Any relation to neurological symptoms remains hypothetical and should be evaluated in cohorts with concurrent clinical phenotyping [31]. A brain-related problem after a long-term COVID-19 infection probably causes 77% of memory fog [32]. These results link the primary function of phosphatidylcholine composition (Calzada et al. 2016) in biological cell membranes, the clinical symptoms of patients with COVID-19 (Xu et al. 2022), and the results tabulated herein. The extracted ion chromatograms shown in Figs. 1 and 2 revealed significantly elevated and dysregulated lipids in the plasma and erythrocytes of COVID-19 patients, consistent with data from healthy volunteers.

Figures 1 and 2 show the extracted ion chromatograms of the most concentrated and dysregulated lipids in plasma and erythrocytes from COVID-19 patients, consistent with data from healthy volunteers.

The fold changes of dysregulated glycerophospholipids (GPLs) in the plasma (Fig. 3) and erythrocytes (Fig. 4) of COVID-19 patients were represented as histograms. Additionally, the fold changes of dysregulated and oxidized lipids in erythrocytes (Fig. 5) were plotted to identify the most affected lipid species within the cellular membrane. Table 5 summarizes the dysregulation factors for the total glycerophospholipid classes in plasma and erythrocytes from healthy controls and COVID-19 patients. Notably, the level of dysregulated lysophosphatidylethanolamines (LPEs) in erythrocytes showed a marked 4.3-fold decrease.

Table 5
The dysregulation factor of the sum of glycerophospholipid classes in the plasma and erythrocytes of COVID-19 patients compared with healthy subjects, n = 30

Dysregulated GPL	Matrix	Healthy, µg/mL	COVID-19, µg/mL	Fold change	*
Sum of PEs (decreased)	Plasma	38.53	18.93	-2.0	↓
Sum of PEs (increased)	Plasma	25.08	43.58	1.7	↑
Sum of PEs (decreased)	Erythrocytes	69.91	35.07	-2.0	↓
Sum of PEs (increased)	Erythrocytes	149.41	247.90	1.7	↑
Sum of LPCs	Plasma	238.15	115.16	-2.1	↓
Sum of PCs	Plasma	359.89	255.76	-1.4	↓
Sum of PCs	Erythrocytes	106.31	47.48	-2.2	↓
Sum of LPEs	Erythrocytes	14.66	3.42	-4.3	↓
Sum of PIs	Erythrocytes	44.82	18.04	-2.5	↓
* Statistical significance, ↑ a significant increase, ↓ a significant decrease					

Glycerophosphatidylinositols (PIs) are bioactive substances essential for nervous system and brain function [33–35]. It has been reported that the level of PI (16:0/20:4) (-*m/z* 857.5) in the postmortem prefrontal cortex of elderly patients with schizophrenia showed a significant decrease [36]. In this study, PI levels decreased significantly, including PI (18:0/20:4) and PI (16:0/20:4). Table 4 shows that the eight quantified PIs are significantly lower in erythrocytes from COVID-19 patients than in control samples. Phosphatidylinositol phosphate kinases have been reported to be activated during viral infection and to promote viral replication [37]. Enhanced phosphatase activity increases LPI 20:4 (-m/z 619.4) due to enzymatic hydrolysis of PI (16:0/20:4) (m/z 857.5) and PI (18:0/20:4) (*m/z* 885.5) (Table 4). Because PIs are essential components of the nervous system, dysregulated PI composition may contribute to memory loss or memory fog [38].

In adults, disrupted arachidonic acid metabolism (C20:4, −*m/z* 303.3) may contribute to neuropsychiatric disorders, including Alzheimer's disease and bipolar disorder, but this was not proven in this study [39]. Evidence suggests that the conversion of arachidonic acid to other bioactive molecules (overexpression or disruption of the AA enzyme cascade) is significantly altered under these conditions. The biological role of arachidonic acid and its metabolites has been studied in the context of various neurodegenerative diseases, including Alzheimer's disease [40].

The formation of a hydroperoxide derivative (-*m/z* 309) from alpha-linolenic acid (C18:3, ALA, -*m/z* 277.2) has been attributed to the enzyme-catalyzed process of a fungus called the manganese lipoxygenase of the rice blast fungus [41]. Liu et al. also reported an enzyme in human recombinant cells, 15-lipoxygenase (type 2), which leads to the formation of 9-hydroperoxy-ALA, among other metabolic products [42]. Herein, the erythrocytes of COVID-19 patients showed an elevated level of 13-hydroxyoctadeca-9,11,15-trienoic acid "13-HOTrE, -*m/z* 293.2" due to the oxidation of ALA. ALA levels increased (Table 4) in the erythrocytes of infected patients due to enhanced hydrolysis of LPE 18:3 (+ *m/z* 476) (Table 3).

Arachidonic acid (C20:4; -m/z 303.3) decreased because epoxidation formed 5-HETE (-m/z 319), which increased significantly, as shown in Table 4. The significant increase in 5-HETE (*-m/z* 319) may partly result from the decrease in arachidonic acid (*-m/z* 303). The lower erythrocyte arachidonic acid signal and higher 5-HETE signal were observed concurrently. Because 5-HETE is generally formed through lipoxygenase-mediated oxygenation of arachidonic acid, these cross-sectional data are compatible with altered arachidonic-acid/oxylipin metabolism but do not establish metabolic flux or enzyme activity. All these metabolic changes support the hypothesis of mental problems in COVID-19 patients.

The fold change values representing the dysregulation of glycerophospholipids (GPLs) in the plasma (depicted in Fig. 3) and erythrocytes (illustrated in Fig. 4) of individuals diagnosed with COVID-19 were graphed in a histogram. Moreover, the fold-change distribution of dysregulated and oxidized lipid species in erythrocytes from COVID-19 patients (depicted in Fig. 5) was quantitatively plotted to delineate the lipid components most profoundly affected within the cellular membrane architecture. The dysregulation factor of the cumulative glycerophospholipid classes in the plasma and erythrocytes of healthy individuals and COVID-19 patients is detailed in Table 5. Notably, the dysregulation factor of lysophosphatidylethanolamines (LPEs) in the erythrocytes exhibited a significant 4.3-fold decrease. The levels of 9-HpOTrE, 5-HETE, and 13-HOTrE were increased in the erythrocytes of infected patients by factors of 3.9, 3.6, and 2.0, respectively (Table 5, Fig. 5). The increase likely reflects infection-driven oxidative stress and inflammation, which activate lipoxygenase/non-enzymatic lipid peroxidation of erythrocyte polyunsaturated fatty acids, generating oxidized linoleic/linolenic acid products.

The contrasting increases and decreases of PEs in plasma and erythrocytes observed in Tables 1–4 are justified by viral-induced stress, compartment-specific adaptation, and oxidative remodeling [43], which collectively generate a disease-specific lipidomic fingerprint associated with COVID-19 clinical severity and neurological sequelae. In plasma, certain PE species are upregulated, possibly reflecting repair or adaptive mechanisms, while others—especially plasmenyl-PEs—decline sharply, likely due to oxidative stress and impaired remodeling pathways. Conversely, erythrocytes show an increase in species such as PE 18:1/22:6, suggesting cellular adaptation to hypoxic and inflammatory environments, while decreases in other LPE species hint at selective enzymatic catabolism [6].

Figures 4 and 5 help us quickly deduce the most dysregulated lipids and the expected distribution pattern in plasma and erythrocytes of COVID-19 patients. Based on these results, the lipidomic signature can help identify SARS-CoV-2 infections. Moreover, imbalanced lipid profiles can indicate harmful effects in COVID-19 patients.

A report published by Taquet in late 2021 showed that approximately 20% of people exposed to COVID-19 infection suffer psychiatric disorders, including anxiety, depression, or insomnia, for three months after recovery [44]. Doubtless, the primary factor in Alzheimer's and psychiatric disorders could be partially attributed to the disturbance of cellular lipid composition. It has been reported that a significant accumulation of PEs results from degenerative stress due to ischemic injury and infarction [44]. The sum of PE (16:0/20:4), PE (18:1/20:4), and PE (16:0/22:4) concentrations in the COVID-19 plasma was significantly increased from 15.2 to 26.5 μg/mL, which corresponds to a 74.5% increase (Table 2). The concentration of total PEs accumulated in COVID-19 plasma, including unsaturated fatty acyl esters at sn-2 of C20:4, C20:5, and C22:6, has reached 64.4 μg/mL, corresponding to a 68.6% increase compared with healthy controls. This up-regulation of certain GPEs supports the assumption of psychiatric disorders and memory fog [44, 45].

Most dramatically downregulated LPCs included LPC O-16:0, LPC 20:5, and LPC 20:3, which showed significant decreases of 3.8–4.8. Lysophosphatidylcholine (LPC) is increasingly recognized as a critical factor positively associated with cardiovascular and neurodegenerative diseases [46]. Plemel et al. observed that the LPC level in mouse cell membranes increased after injury healing. This increase was interpreted as a defense mechanism aimed at restoring brain health [47]. The top three PEs that showed upregulation included PE (18:1/20:4), PE (18:0/20:5), and PE (16:0/20:4). The results showed a significant increase by a factor ranging from 2.1 to 2.8 (Fig. 3). These results shed light on the importance of LPCs and PEs as associated markers with SARS-CoV-2 viral infections.

Lopez et al. investigated the lipidomic profile of plasma from COVID-19 patients 2 years after recovery [48]. They concluded that lipid dysregulation was present in the recently infected cases. Lopez et al. attributed some persistent illnesses, especially musculoskeletal problems, to lipid dysregulation due to previous SARS-CoV-2 infection and recovery. Our results suggest that COVID-19 patients are associated with a neuropsychiatric syndrome due to metabolic dysregulation of some lipids, which play a vital role in mental health. Based on these results, consuming foods rich in omega-3 fatty acids may be helpful [49].

3.3 Multivariate statistical analysis

Principal component analysis (PCA) of dysregulated lipids in plasma and erythrocytes (Fig. 6) showed clear separation of plot scores between healthy subjects and COVID-19 patients. The scores were well separated overall using data from down- and upregulated lipid entities. PCA was applied to the quantified lipidomic data acquired from plasma and erythrocyte samples of both COVID-19 patients and matched healthy subjects. PCA is a powerful unsupervised statistical technique that reduces the dimensionality of complex datasets by identifying patterns and grouping samples based on primary sources of variance, without pre-assumed class labels. In this study, PCA enabled visualization of

distinct lipidomic alterations characterizing clinical COVID-19, yielding clear separation between patient and control cohorts on the PCA score plot, with healthy and COVID-19 cases forming non-overlapping clusters.

The analysis included scores derived from both upregulated and downregulated phospholipid species, maximizing sensitivity for disease discrimination. Each data point in the PCA plot represents an individual and summarizes concentrations across major dysregulated lipid species, including PE, PC, PI, LPE, and LPC. Notably, key lipids driving the group separation included the sharp increase in erythrocyte PE 18:1/22:6 and significant reductions in plasma plasmalogen-PEs, LPCs, and PIs. The PCA score plot suggested partial clustering of hospitalized COVID-19 patients apart from healthy controls, consistent with group-associated variation in the measured lipid profiles. Because PCA is an unsupervised exploratory method, the observed pattern requires confirmation using appropriately validated predictive analyses and an independent cohort

PCA not only corroborates the univariate findings but also uncovers complex interrelationships among lipids that single-variable tests may miss. The strong group separation suggests underlying metabolic disruptions with potential clinical relevance, supporting the idea that SARS-CoV-2 induces comprehensive membrane lipid remodeling detectable by LC-MS-based approaches and suitable for developing lipid biomarker panels.

3.4 Analytical and Clinical Value of Paired Plasma–Erythrocyte LC–MS^n Lipidomics

This study shows that paired plasma–erythrocyte LC–MS^n lipidomic profiling can reveal compartment-specific membrane remodeling and oxidative injury that plasma-only analyses may overlook. The combined evaluation of plasma and erythrocyte lipidomes by LC–ion-trap MS^n identified a coordinated but biologically distinct signature of COVID-19-associated lipid dysregulation. The analytical value of the workflow extends beyond detecting differences in lipid abundance, as lipid assignments were supported by chromatographic retention behavior, diagnostic multistage fragmentation, acquisition in positive- and negative-ion modes, class-matched internal standards, and comparison with NIST2020 and MoNA spectral resources. This integrated approach revealed a convergent oxidative-stress phenotype characterized by depletion of plasma antioxidant plasmenyl-phosphatidylethanolamines and lysophosphatidylcholines, accompanied by increased erythrocyte oxidized fatty-acid mediators, including 9-HpOTrE, 5-HETE, and 13-HOTrE. In parallel, the data demonstrated erythrocyte-specific remodeling of phosphatidylethanolamines, phosphatidylcholines, lysophosphatidylethanolamines, and phosphatidylinositols. In particular, the increased abundance of erythrocyte PE 18:1/22:6, together with pronounced decreases in LPEs and PIs, indicates that erythrocytes provide biologically complementary information not fully represented by circulating plasma lipids. Collectively, this paired plasma–erythrocyte mass-spectrometric approach provides an exploratory framework for identifying compartment-specific lipid candidates for subsequent targeted verification. Future studies should evaluate these candidates using analytically validated assays in independent, clinically well-characterized longitudinal cohorts before considering their potential role in patient stratification or monitoring.

Nevertheless, these findings are exploratory and require confirmation with quantitative LC–MS/MS assays using authentic reference standards, followed by validation in an independent cohort, before proposing any diagnostic or prognostic application. A confirmation panel incorporating erythrocyte PE 18:1/22:6, selected plasma LPC and plasmenyl-PE species, and erythrocyte oxylipins represents a practical next step toward clinically deployable LC–MS/MS testing, provided that analytical transferability, pre-analytical stability, diagnostic performance, and external reproducibility are rigorously established.

Collectively, this paired plasma–erythrocyte mass-spectrometric approach provides an exploratory framework for identifying compartment-specific lipid candidates for subsequent targeted verification. Future studies should evaluate these candidates using analytically validated assays in independent, clinically well-characterized longitudinal cohorts before considering their potential role in patient stratification or monitoring. Integrating quantitative LC-IT-MS^n data with multivariate statistical analysis (PCA) shows that SARS-CoV-2 infection induces coordinated disturbances across glycerophospholipids (GPLs), plasmalogens, lysophospholipids, and oxylipins. These alterations, summarized in Tables 1–4 and visualized in Figs. 1–5, offer mechanistic insight into the neurological, hematological, and inflammatory manifestations observed clinically.

Tables 1–3 highlight the most significantly altered GPL species in plasma and erythrocytes. In plasma, GPLs containing arachidonic acid (AA) at the sn-2 position exhibited marked shifts. PC (18:0/18:2) and PC (16:0/20:3) decreased by 24.8%, accounting for 38% of total down-regulated GPLs (Table 2). Conversely, PE (16:0/20:4) and PE (18:1/20:4) increased by 90.4%, indicating selective upregulation of AA-containing PEs. In erythrocytes, PE (18:1/22:6) showed the most pronounced accumulation, rising 1.5-fold to 126.2 µg/mL (Table 3). This enrichment of docosahexaenoic acid (DHA) containing PEs suggests compensatory remodeling of erythrocyte membranes under oxidative and inflammatory stress. Figures 1 and 2 corroborate these findings, showing intensified peaks in the extracted-ion chromatogram for PE (18:1/22:6) and other dysregulated GPLs.

Plasmalogens, particularly plasmenyl-PEs, were reduced by 52.7% in plasma (Table 2). These lipids serve as endogenous antioxidants because their vinyl-ether bond preferentially absorbs oxidative damage. Their depletion indicates heightened oxidative stress and diminished membrane protection. The reduction of PE-P (16:0/22:6), PE-P (18:0/20:4), and related species aligns with the elevated oxylipins observed in Fig. 5.

Lysophosphatidylcholines (LPCs) were extensively downregulated in plasma, with LPC 20:5 and LPC 20:3 decreasing by approximately fourfold (Table 2). LPCs are essential for membrane turnover and inflammatory signaling; thus, their depletion suggests impaired phospholipase activity and disrupted lipid signaling. In contrast, erythrocyte LPC 15:0 increased significantly (Table 3), indicating compartment-specific remodeling. Lysophosphatidylethanolamines (LPEs) decreased dramatically by 4.3-fold in erythrocytes (Table 5), reflecting impaired membrane repair pathways. Figure 4 illustrates these erythrocyte-specific fold changes. Oxidized fatty acids—9-HpOTrE, 5-HETE, and 13-HOTrE—increased by 3.9-, 3.6-, and 2.0-fold, respectively (Table 4). The higher oxylipin signals are compatible with altered lipid oxidation and inflammatory lipid metabolism in the COVID-19 group, as visualized in Fig. 5.

The parallel reduction in erythrocyte AA and increase in AA-derived oxylipins suggest accelerated lipoxygenase activity. This shift may contribute to neuroinflammation, given the role of AA metabolites in modulating neuronal excitability.

Erythrocytes exhibited profound lipid remodeling, with significant increases in PC (16:1/16:1), PC (18:0/18:1), and PC (20:4/20:5) (Table 3). These changes likely reflect adaptive responses to oxidative stress that preserve membrane integrity. However, decreased levels of PC (15:0/20:5) and PC (16:0/18:3) indicate selective depletion of certain fatty acid species. Figure 4 shows the fold-change distribution of erythrocyte GPLs, highlighting the imbalance between upregulated and downregulated species. Such remodeling may impair erythrocyte deformability, exacerbate hypoxia, and contribute to microvascular complications.

Dysregulation of neuron-relevant lipids, including PEs, PIs, and LPCs, provides a possible biochemical explanation for post-COVID neuropsychiatric symptoms. Table 4 shows significant reductions in PI (16:0/20:4) and PI (18:0/20:4), mirroring patterns observed in neurodegenerative disorders such as schizophrenia.

Plasmalogen depletion further compromises neuronal protection against oxidative stress. Given that 77% of long-COVID patients report memory fog, these lipidomic disturbances offer a plausible mechanistic explanation.

The Principal Component Analysis (PCA) score plot (Fig. 6) shows complete separation between COVID-19 and healthy subjects, confirming that the lipidomic alterations are systematic and disease-specific. This statistical distinction underscores the robustness of the lipidomic signature and supports its potential use as a candidate feature for targeted validation.

Table 5 summarizes the dysregulation factors across lipid classes, highlighting consistent disturbances in GPLs, plasmalogens, LPCs, and LPEs. These coordinated shifts suggest that lipidomic profiling may serve as a valuable clinical tool to assess disease severity, monitor recovery, and identify patients at risk for neurological complications. These identified features may be prioritized for analytical confirmation and mechanistic investigation.

Collectively, the results presented in Tables 1–4 and Figs. 1–5 reveal a COVID-19-specific lipidomic signature characterized by oxidative stress, membrane remodeling, and dysregulation of neuronal-critical lipid pools. These findings provide mechanistic insight into the neurological and hematological manifestations of COVID-19 and highlight Lipidomics' potential as a biomarker platform for clinical management.

3.5 Multiple-testing and effect-size analysis:

Across the tabulated lipid panels, the direction and magnitude of the reported group differences remained robust after FDR adjustment of the p-values reconstructed from the available summary statistics. All 41 plasma glycerophospholipid species, all 43 erythrocyte glycerophospholipid species, and all 15 erythrocyte oxylipin/phosphatidylinositol-related analytes retained an FDR-adjusted q-value below 0.05. The median absolute Hedges' g was 1.21 for plasma glycerophospholipids, 1.33 for erythrocyte glycerophospholipids, and 0.73 for erythrocyte oxylipins/phosphatidylinositols. Large standardized effects (absolute Hedges' g ≥ 0.80) were observed for 38/41 plasma glycerophospholipids and 36/43 erythrocyte glycerophospholipids, whereas 5/15 oxylipin/phosphatidylinositol-related analytes met this threshold (Table S1).

The most pronounced plasma changes were reductions in LPC P-18:0 (COVID/control fold change, 0.26; Hedges' g = − 2.05; FDR $q = 8.46 \times 10^{-9}$), LPC 16:0 (0.56; g = − 1.90; $q = 1.01 \times 10^{-8}$), and LPC 18:2 (0.34; g = − 1.89; $q = 1.15 \times 10^{-7}$). Among erythrocyte glycerophospholipids, the largest effects included a reduction in LPE 18:1 (0.13; g = − 2.68; $q = 3.36 \times 10^{-12}$), an increase in LPE 22:6 (21.88; g = 2.63; $q = 2.12 \times 10^{-10}$), an increase in PE 18:0/18:1 (1.89; g = 2.52; $q = 6.99 \times 10^{-12}$), and a reduction in PC 18:0/20:5 (0.42; g = − 2.39; $q = 6.99 \times 10^{-12}$). In the

erythrocyte oxylipin/phosphatidylinositol panel, the strongest standardized reductions were observed for LPI 18:0 (0.27; g = − 1.13; q = 0.0015), PI 16:0/18:2 (0.28; g = − 1.00; q = 0.0025), and PI 18:0/20:4 (0.43; g = − 0.97; q = 0.0026) (Table S2).

Together, the FDR-adjusted analysis supports broad, quantitatively substantial remodeling of plasma and erythrocyte lipid composition in the hospitalized COVID-19 group. The largest effects were concentrated among lysophospholipids and selected membrane phospholipids, while the oxylipin/phosphatidylinositol panel showed more moderate but still statistically robust effects. These data should be interpreted as associations in this exploratory case–control cohort and require confirmation in an independent cohort before being proposed as diagnostic or candidate features for targeted validation.

3.6 Supplementary figure

Figure S1. Standardized effect sizes for the ten largest COVID-19–control lipid differences in each analytical panel. Hedges' g was calculated from tabulated means and standard deviations for 30 hospitalized COVID-19 patients and 30 healthy controls. Positive values (red) indicate higher concentrations in the COVID-19 group; negative values (blue) indicate lower concentrations. Features are ranked by absolute Hedges' g within each panel.

COVID-19 versus control comparisons for tabulated lipid species: fold changes, log2 fold changes, Hedges' g, reconstructed Welch-test p-values, and Benjamini–Hochberg FDR-adjusted q-values.

4 Conclusion

In conclusion, this exploratory case–control study used paired plasma and erythrocyte lipidomic profiling by optimized LC–ion-trap MS/MS to identify a distinct COVID-19-associated pattern of membrane lipid remodeling and oxidative lipid injury. The analytical phase used rigorous untargeted lipidomic characterization of plasma and erythrocytes, with optimized extraction under inert conditions to prevent auto-oxidation and high-sensitivity LC-MS/MS analysis on a linear ion trap mass spectrometer with systematic calibration. This approach was applied to samples from 30 COVID-19 patients and 30 matched healthy controls to reliably quantify and identify lipid species, while principal component analysis validated group separation and reproducibility. The primary objective was to uncover SARS-CoV-2-induced metabolic disorders in membrane lipids and to investigate their link to neuropsychiatric symptoms. The study found distinctive dysregulation: a 1.5-fold increase in erythrocyte phosphatidylethanolamine, lower plasma LPC signals, lower erythrocyte PI signals, and higher erythrocyte oxidized lipid mediator signals. For example, erythrocyte PE 18:1/22:6 was higher in the COVID-19 group (126.15 µg/mL versus 82.46 µg/mL), whereas plasma PC 16:0/20:3 was lower (78.79 µg/mL versus 102.49 µg/mL). In this exploratory case–control study, the observed differences in plasma and erythrocyte lipids are consistent with altered membrane lipid remodeling and increased oxidized lipid mediator abundance in hospitalized COVID-19 patients. Although several affected lipid classes have recognized roles in membrane biology and inflammatory signaling, these data do not establish causal mechanisms, membrane functional impairment, or cognitive and psychiatric consequences. These lipid features should therefore be regarded as candidate targets for analytical confirmation and evaluation in independent, clinically characterized longitudinal cohorts before considering them for targeted validation or clinical applications [50].

Abbreviations

AA
arachidonic acid
ALA
alpha-linolenic acid
ARDS
acute respiratory distress syndrome
C18:2
linoleic acid
C18:3
alpha-linolenic acid
C20:0
arachidic acid (eicosanoic acid)
C20:4
arachidonic acid
COVID-19
coronavirus disease 2019
CP
COVID-19 plasma samples

CR
COVID-19 red blood cell samples
DSR
Deanship of Scientific Research
EDTA
ethylenediaminetetraacetic acid
ESI
electrospray ionisation
FreeStyle
data visualisation software
GPL
glycerophospholipid
GPLs
glycerophospholipids
HDL
high-density lipoprotein
HETE
hydroxyeicosatetraenoic acid
HOTrE
hydroxyoctadecatrienoic acid
HP
healthy plasma samples
HpOTrE
hydroperoxy-octadecatrienoic acid
HR
healthy red blood cell samples
IS
internal standard
IT-MS
ion-trap mass spectrometry
KAU
King Abdulaziz University
kV
kilovolts
LA
linoleic acid
LC-IT-MS^n
liquid chromatography coupled to linear ion-trap tandem mass spectrometry
LC-MS/MS
liquid chromatography–tandem mass spectrometry
LPC
lysophosphatidylcholine
LPE
lysophosphatidylethanolamine
LPI
lysophosphatidylinositol
m/z
mass-to-charge ratio
mL
millilitres
min
minutes
MoNA
MassBank of North America

MVSP
Multivariate Statistical Package
µg/mL
micrograms per millilitre
µL
microlitres
ng/µL
nanograms per microlitre
ng/mL
nanograms per millilitre
NIST
National Institute of Standards and Technology
PC
phosphatidylcholine
PCA
principal component analysis
PCR
polymerase chain reaction
PE
phosphatidylethanolamine
PE(P)
plasmenyl-phosphatidylethanolamine
PE-P
plasmenyl-phosphatidylethanolamine
PI
phosphatidylinositol
PL
phospholipid
PTFE
polytetrafluoroethylene
PUFA
polyunsaturated fatty acid
RBCs
red blood cells
rpm
revolutions per minute
SARS-CoV-2
severe acute respiratory syndrome coronavirus 2
SD
standard deviation
tR
retention time
V
volts
v/v
volume per volume
w/v
weight per volume
WHO
World Health Organization.

Declarations

Author contributions Alaa Khedr: Writing – original draft, Project administration, Methodology, Data curation, Writing – review & editing, Supervision, Conceptualization. **Ahdab N. Khayyat :** Writing – original draft, Project administration, Methodology, Data curation. **Ahmed K.**

Kammoun : Methodology, Formal analysis, Data curation.

Funding The Deanship of Scientific Research (DSR) at King Abdulaziz University (KAU), Jeddah, Saudi Arabia, has funded this project under Grant no.: G-280-166-1442.

Declaration of competing interest

The authors declare that they have no known competing financial interests or personal relationships that could have appeared to influence the work reported in this paper.

Data Availability: The datasets generated and/or analyzed during the current study are not publicly available because they include de-identified human participant data and are subject to institutional ethical restrictions, but they are available from the corresponding author upon reasonable request, subject to approval by the relevant ethics committee and applicable institutional data-sharing requirements.

Ethical Approval and accordance: The study protocol involving human participants and blood-sample collection was approved by the King Abdulaziz University Hospital Ethics Committee, King Abdulaziz University, Jeddah, Saudi Arabia, under approval reference number 408-20. The institution is registered with the National Committee of Bioethics under registration number HA-02-J-008. The study was conducted in accordance with the ethical standards and guidelines of the approving ethics committee, the applicable institutional regulations, and the principles of the Declaration of Helsinki [51].

Consent for publication: Freely-given, written informed consent to participate in the study was obtained from all participants before their inclusion in the study.

Competing interests: The authors declare no competing interests.

References

1. World Health Organization. Public health surveillance for COVID-19: interim guidance, Surveillance, case investigation and epidemiological protocols. 2022.
2. World Health Organization. WHO COVID-19: Case Definitions, Updated in Public health surveillance for COVID-19. 2022.
3. Shen B, Yi X, Sun Y, Bi X, Du J, Zhang C, et al. Proteomic and Metabolomic Characterization of COVID-19 Patient Sera. Cell. 2020;182(1):59–e7215. 10.1016/j.cell.2020.05.032.
4. Varga Z, Flammer AJ, Steiger P, Haberecker M, Andermatt R, Zinkernagel AS, et al. Endothelial cell infection and endotheliitis in COVID-19. Lancet (London England). 2020;395(10234):1417–8. 10.1016/s0140-6736(20)30937-5.
5. Surma S, Banach M, Lewek J. COVID-19 and lipids. The role of lipid disorders and statin use in the prognosis of patients with SARS-CoV-2 infection. Lipids Health Dis. 2021;20(1):141. 10.1186/s12944-021-01563-0.
6. Wei J, Liu X, Xiao W, Lu J, Guan L, Fang Z, et al. Phospholipid remodeling and its derivatives are associated with COVID-19 severity. J Allergy Clin Immunol. 2023;151(5):1259–68. 10.1016/j.jaci.2022.11.032.
7. Xu K, Nagy PD. RNA virus replication depends on enrichment of phosphatidylethanolamine at replication sites in subcellular membranes. Proc Natl Acad Sci U S A. 2015;112(14):E1782–91. 10.1073/pnas.1418971112.
8. Yan B, Chu H, Yang D, Sze K-H, Lai P-M, Yuan S, et al. Characterization of the Lipidomic Profile of Human Coronavirus-Infected Cells: Implications for Lipid Metabolism Remodeling upon Coronavirus Replication. Viruses. 2019;11(1). 10.3390/v11010073.
9. Hoebinger C, Rajcic D, Hendrikx T. Oxidized Lipids: Common Immunogenic Drivers of Non-Alcoholic Fatty Liver Disease and Atherosclerosis. Front Cardiovasc Med. 2021;8:824481. 10.3389/fcvm.2021.824481.
10. Oliw EH, Aragó M, Chen Y, Jernerén F. A new class of fatty acid allene oxide formed by the DOX-P450 fusion proteins of human and plant pathogenic fungi, C. immitis and Z. tritici. J Lipid Res. 2016;57(8):1518–28. 10.1194/jlr.M068981.
11. Parthasarathy S, Raghavamenon A, Garelnabi MO, Santanam N. Oxidized low-density lipoprotein. Methods Mol Biol. 2010;610:403–17. 10.1007/978-1-60327-029-8_24.
12. André A, Juanéda P, Sébédio JL, Chardigny JM. Plasmalogen metabolism-related enzymes in rat brain during aging: influence of n-3 fatty acid intake. Biochimie. 2006;88(1):103–11. 10.1016/j.biochi.2005.06.010.
13. Brites P, Waterham HR, Wanders RJ. Functions and biosynthesis of plasmalogens in health and disease. Biochim Biophys Acta. 2004;1636(2–3):219–31. 10.1016/j.bbalip.2003.12.010.
14. Pike DP, McGuffee RM, Geerling E, Albert CJ, Hoft DF, Shashaty MGS, et al. Plasmalogen Loss in Sepsis and SARS-CoV-2 Infection. Front Cell Dev Biol. 2022;10. 10.3389/fcell.2022.912880.

15. Khedr A, Khayat MT, Khayyat AN. A new approach for characterization of phosphatidylcholines and lysophosphatidylcholine in human plasma. Bioanalysis. 2020;12(3):191–204. 10.4155/bio-2019-0280.
16. Kuypers FA. Membrane lipid alterations in hemoglobinopathies. Hematol Am Soc Hematol Educ Program. 2007;68–73. 10.1182/asheducation-2007.1.68.
17. Tang HY, Wang CH, Ho HY, Wu PT, Hung CL, Huang CY, et al. Lipidomics reveals accumulation of the oxidized cholesterol in erythrocytes of heart failure patients. Redox Biol. 2018;14:499–508. 10.1016/j.redox.2017.10.020.
18. Myers DS, Ivanova PT, Milne SB, Brown HA. Quantitative analysis of glycerophospholipids by LC-MS: acquisition, data handling, and interpretation. Biochim Biophys Acta. 2011;1811(11):748–57. 10.1016/j.bbalip.2011.05.015.
19. Pulfer M, Murphy RC. Electrospray mass spectrometry of phospholipids. Mass Spectrom Rev. 2003;22(5):332–64. https://doi.org/10.1002/mas.10061.
20. Khedr A, El-Hay SS, Kammoun KA. Multi-Steps Fragmentation-Ion Trap Mass Spectrometry Coupled to Liquid Chromatography Diode Array System for Investigation of Olaparib Related Substances. Molecules. 2019;24(5). 10.3390/molecules24050843.
21. Bligh EG, Dyer WJ. A rapid method of total lipid extraction and purification. Can J Biochem Physiol. 1959;37(8):911–7. 10.1139/o59-099.
22. Rose HG, Oklander M. Improved procedure for the extraction of lipids from human erythrocytes. J Lipid Res. 1965;6(3):428–31. https://doi.org/10.1016/S0022-2275(20)39314-7.
23. Rasool G, Riaz M, Abbas M, Fatima H, Qamar MM, Zafar F, et al. COVID-19: Clinical laboratory diagnosis and monitoring of novel coronavirus infected patients using molecular, serological and biochemical markers: A review. Int J Immunopathol Pharmacol. 2022;36:03946320221115316. 10.1177/03946320221115316.
24. COVID-19 Treatment Guidelines Panel. Coronavirus Disease 2019, National Institutes of Health. Available at https://www.covid19treatmentguidelines.nih.gov/. Accessed September 30, 2022.
25. Zhang Z, Karu N, Kindt A, Singh M, Lamont L, van Gammeren AJ, et al. Association of Altered Plasma Lipidome with Disease Severity in COVID-19 Patients. Biomolecules. 2024;14(3). 10.3390/biom14030296.
26. Welch BL. On the Comparison of Several Mean Values: An Alternative Approach. Biometrika. 1951;38(3/4):330–6. 10.2307/2332579.
27. Benjamini Y, Hochberg Y. Controlling the False Discovery Rate: A Practical and Powerful Approach to Multiple Testing. J Roy Stat Soc: Ser B (Methodol). 1995;57(1):289–300. 10.1111/j.2517-6161.1995.tb02031.x.
28. Hedges LV. Distribution Theory for Glass's Estimator of Effect size and Related Estimators. J Educational Stat. 1981;6(2):107–28. 10.3102/10769986006002107.
29. Khedr A, El-Hay SSA, Kammoun AK. Multi-Steps Fragmentation-Ion Trap Mass Spectrometry Coupled to Liquid Chromatography Diode Array System for Investigation of Olaparib Related Substances. Molecules. 2019;24(5):843.
30. Rose HG, Oklander M. Improved procedure for the extraction of lipids from human erythrocytes. J Lipid Res. 1965;6(3):428–31. https://doi.org/10.1016/S0022-2275(20)39314-7.
31. Calzada E, Onguka O, Claypool SM. Phosphatidylethanolamine Metabolism in Health and Disease. Int Rev Cell Mol Biol. 2016;321:29–88. 10.1016/bs.ircmb.2015.10.001.
32. Xu E, Xie Y, Al-Aly Z. Long-term neurologic outcomes of COVID-19. Nat Med. 2022;28(11):2406–15. 10.1038/s41591-022-02001-z.
33. Balakrishnan SS, Basu U, Raghu P. Phosphoinositide signalling in Drosophila. Biochim Biophys Acta - Mol Cell Biol Lipids. 2015;1851(6):770–84. https://doi.org/10.1016/j.bbalip.2014.10.010.
34. Balla T. Phosphoinositides: tiny lipids with giant impact on cell regulation. Physiol Rev. 2013;93(3):1019–137. 10.1152/physrev.00028.2012.
35. Raghu P, Joseph A, Krishnan H, Singh P, Saha S. Phosphoinositides: Regulators of Nervous System Function in Health and Disease. Front Mol Neurosci. 2019;12:208. 10.3389/fnmol.2019.00208.
36. Matsumoto J, Nakanishi H, Kunii Y, Sugiura Y, Yuki D, Wada A, et al. Decreased 16:0/20:4-phosphatidylinositol level in the post-mortem prefrontal cortex of elderly patients with schizophrenia. Sci Rep. 2017;7(1):45050. 10.1038/srep45050.
37. Beziau A, Brand D, Piver E. The Role of Phosphatidylinositol Phosphate Kinases during Viral Infection. Viruses. 2020;12(10). 10.3390/v12101124.
38. Dickson EJ. Recent advances in understanding phosphoinositide signaling in the nervous system. F1000Res. 2019;8. 10.12688/f1000research.16679.1.
39. Rapoport SI. Arachidonic acid and the brain. J Nutr. 2008;138(12):2515–20. 10.1093/jn/138.12.2515.
40. Kursun O, Karatas H, Bariskaner H, Ozturk S. Arachidonic Acid Metabolites in Neurologic Disorders. CNS Neurol Disord – Drug Targets. 2022;21(2):150–9. http://dx.doi.org/10.2174/1871527320666210512013648.

41. Wennman A, Jernerén F, Magnuson A, Oliw EH. Expression and characterization of manganese lipoxygenase of the rice blast fungus reveals prominent sequential lipoxygenation of α-linolenic acid. Arch Biochem Biophys. 2015;583:87–95. 10.1016/j.abb.2015.07.014.
42. Liu M, Chen P, Véricel E, Lelli M, Béguin L, Lagarde M, et al. Characterization and biological effects of di-hydroxylated compounds deriving from the lipoxygenation of ALA. J Lipid Res. 2013;54(8):2083–94. https://doi.org/10.1194/jlr.M035139.
43. Xue M, Zhang T, Cheng ZJ, Guo B, Zeng Y, Lin R, et al. Effect of a Functional Phospholipid Metabolome-Protein Association Pathway on the Mechanism of COVID-19 Disease Progression. Int J Biol Sci. 2022;18(12):4618–28. 10.7150/ijbs.72450.
44. Taquet M, Luciano S, Geddes JR, Harrison PJ. Bidirectional associations between COVID-19 and psychiatric disorder: retrospective cohort studies of 62 354 COVID-19 cases in the USA. The Lancet Psychiatry. 2021;8(2):130 – 40. doi: 10.1016/S2215-0366(20)30462-4.
45. Wellner N, Diep TA, Janfelt C, Hansen HS. N-acylation of phosphatidylethanolamine and its biological functions in mammals. Biochim Biophys Acta. 2013;1831(3):652–62. 10.1016/j.bbalip.2012.08.019.
46. Law SH, Chan ML, Marathe GK, Parveen F, Chen CH, Ke LY. An Updated Review of Lysophosphatidylcholine Metabolism in Human Diseases. Int J Mol Sci. 2019;20(5). 10.3390/ijms20051149.
47. Plemel JR, Michaels NJ, Weishaupt N, Caprariello AV, Keough MB, Rogers JA, et al. Mechanisms of lysophosphatidylcholine-induced demyelination: A primary lipid disrupting myelinopathy. Glia. 2018;66(2):327–47. 10.1002/glia.23245.
48. López-Hernández Y, Oropeza-Valdez JJ, García Lopez DA, Borrego JC, Murgu M, Valdez J, et al. Untargeted analysis in post-COVID-19 patients reveals dysregulated lipid pathways two years after recovery. Front Mol Biosci. 2023;10. 10.3389/fmolb.2023.1100486.
49. Rizliya V, Mendis E. Biological, Physical, and Chemical Properties of Fish Oil and Industrial Applications. In: Kim S-K, editor. Seafood Processing By-Products: Trends and Applications. New York, NY: Springer New York; 2014. pp. 285–313.
50. Ou F-S, Michiels S, Shyr Y, Adjei AA, Oberg AL. Biomarker Discovery and Validation: Statistical Considerations. J Thorac Oncol. 2021;16(4):537–45. https://doi.org/10.1016/j.jtho.2021.01.1616.
51. Association WM, World Medical Association Declaration of Helsinki: Ethical Principles for Medical Research Involving Human Participants, Ahmed K. JAMA. 2025;333(1):71 – 4. doi: 10.1001/jama.2024.21972. Authors and Affiliations Alaa Khedr[1,2], Ahdab N. Khayyat[a], Ahmed K Kammoun[1,2] Alaa Khedr khedr@kau.edu.sa https://orcid.org/0000-0003-1057-7455 Ahdab N. Khayyat ankhayyat@kau.edu.sa https://orcid.org/0000-0001-5374-3017 Ahmed K. Kammoun akammoun@kau.edu.sa https://orcid.org/0000-0003-2410-8529 [1] *Department of Pharmaceutical Chemistry, Faculty of Pharmacy, King Abdulaziz University, P.O. Box 80260, Jeddah 21589, Saudi Arabia* [2] *King Fahd Medical Research Center, King Abdulaziz University, P.O. Box 80216, Jeddah 21589, Saudi Arabia* Corresponding author Alaa Khedr, akhedr@kau.edu.sa.

Figures

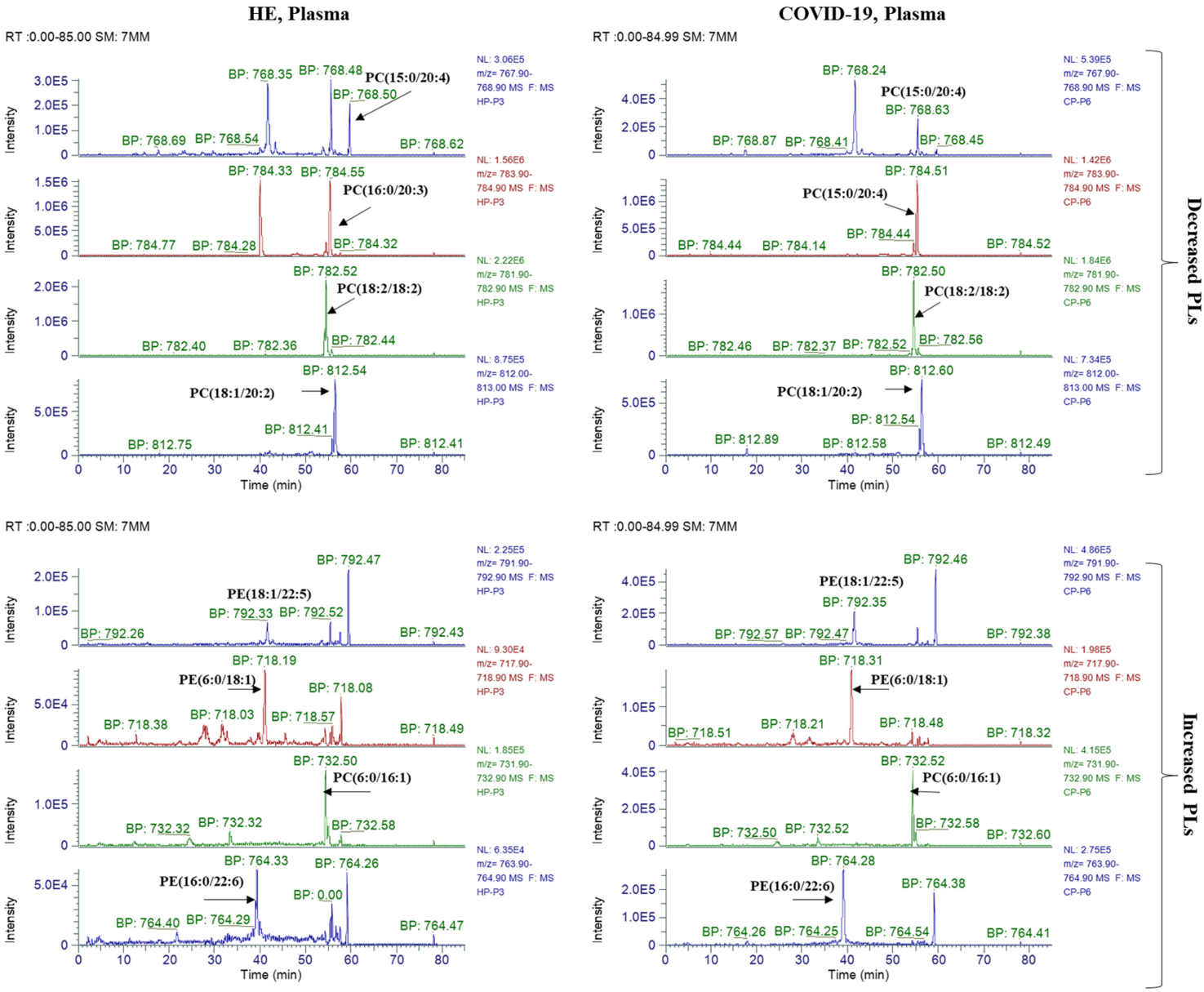


Figure 1

Representative extracted ion chromatogram of selected PLs with relatively high levels that were significantly dysregulated in COVID-19 plasma.

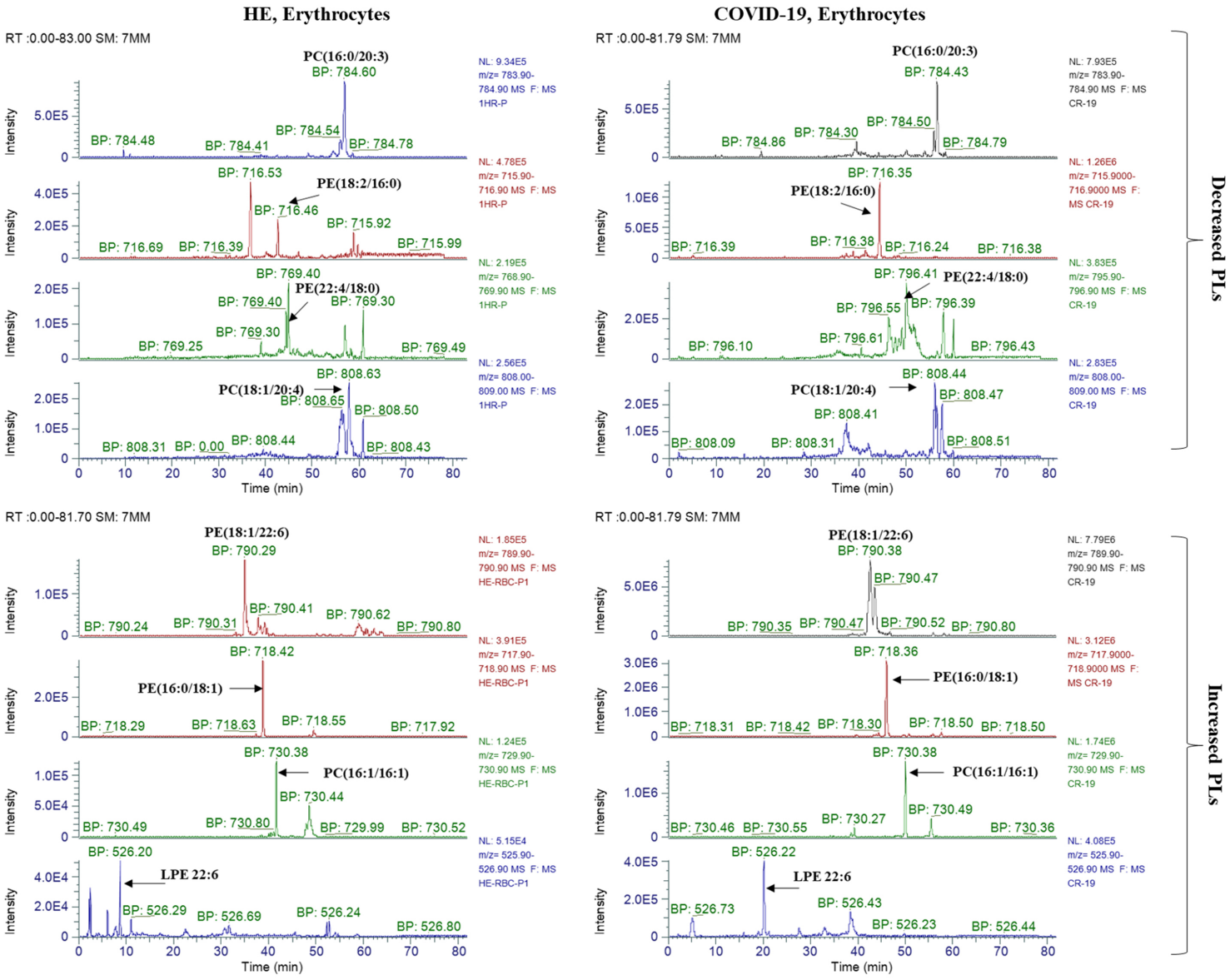


Figure 2

Representative extracted ion chromatogram of selected PLs with relatively high levels that were significantly dysregulated in COVID-19 erythrocytes.

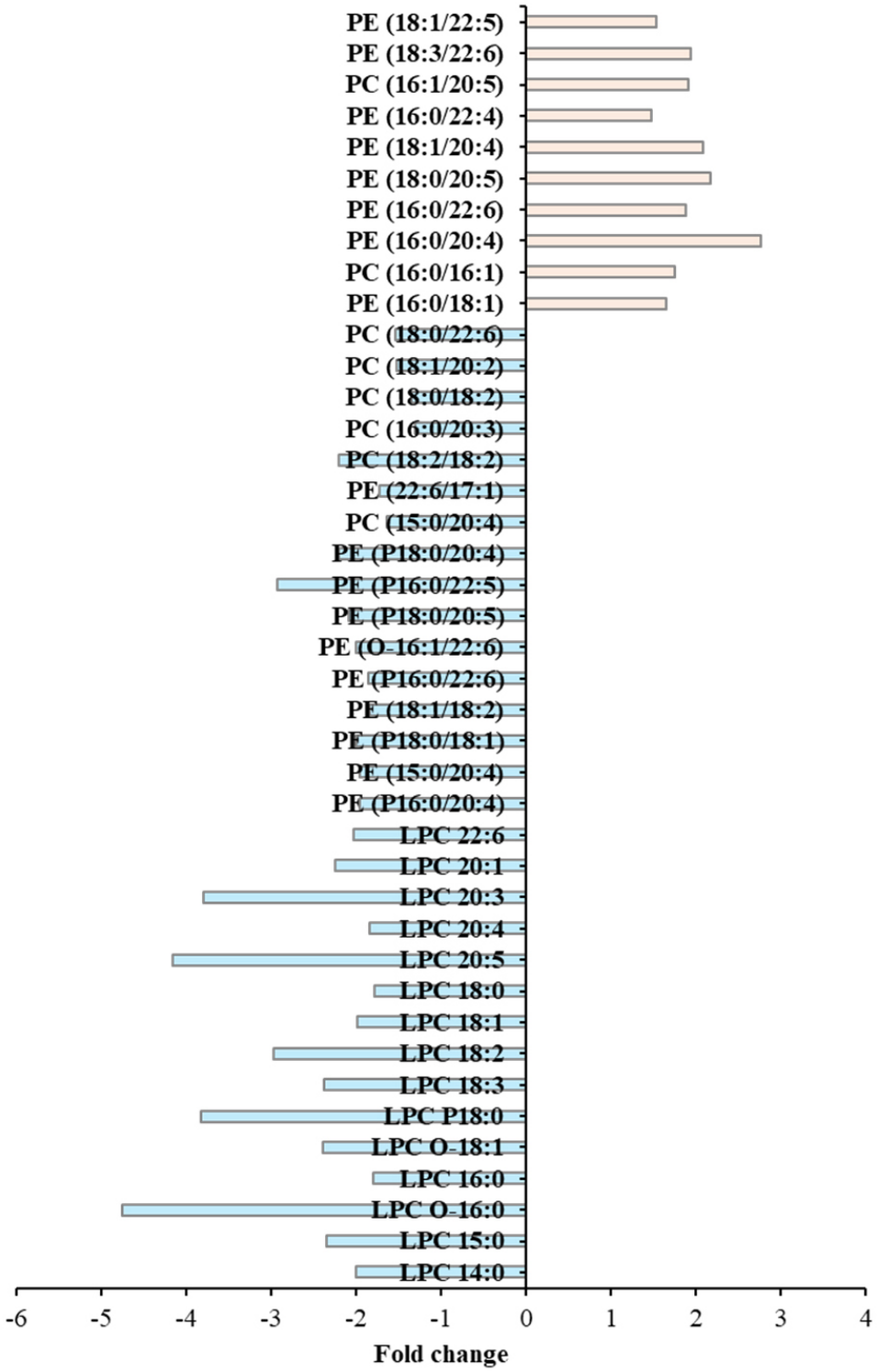


Figure 3

Fold change in glycerophospholipid concentrations in the plasma of COVID-19 patients versus healthy volunteers, n = 30.

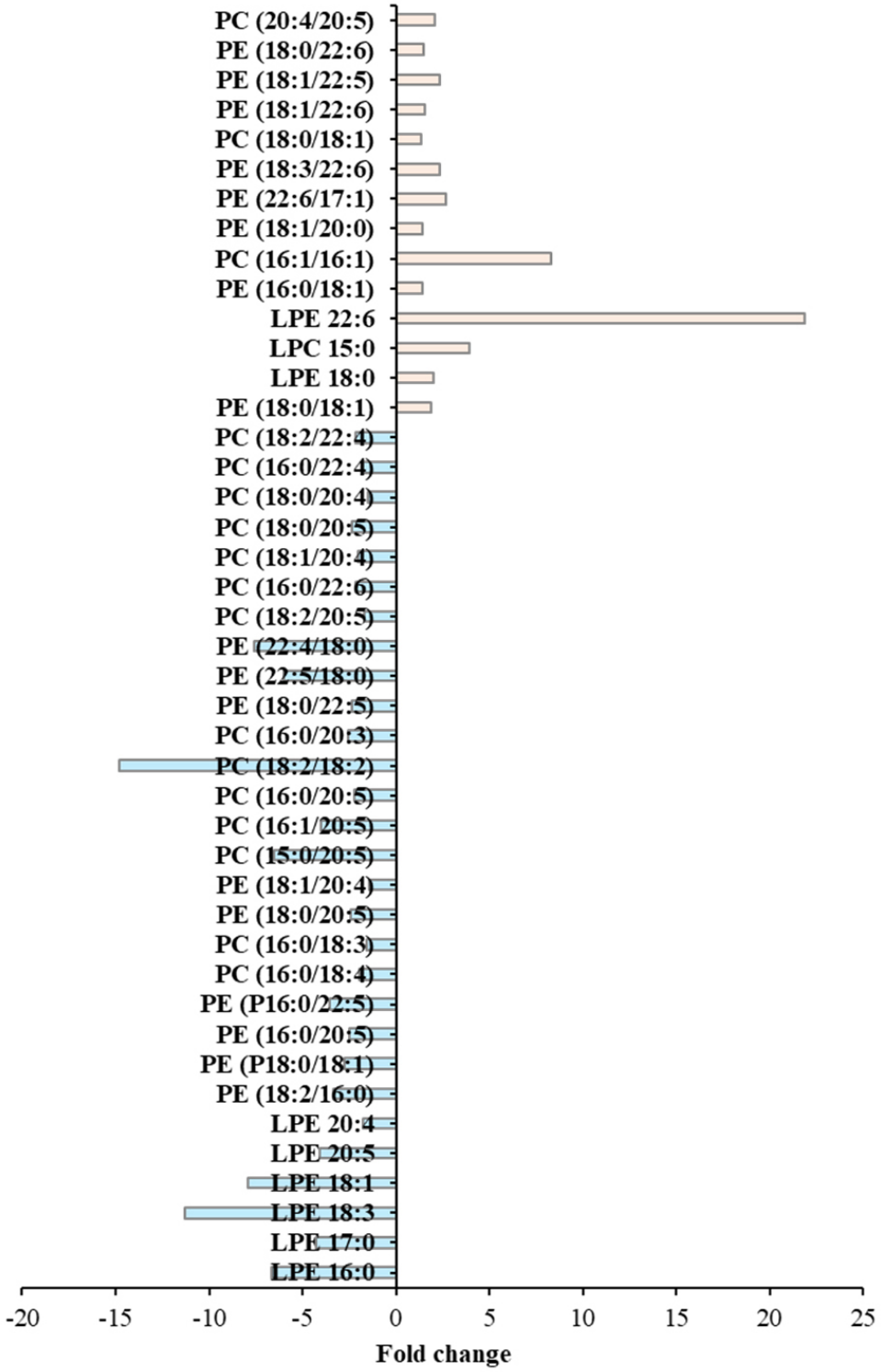


Figure 4

Fold change in glycerophospholipid concentrations in erythrocytes of COVID-19 patients versus healthy volunteers, n = 30.

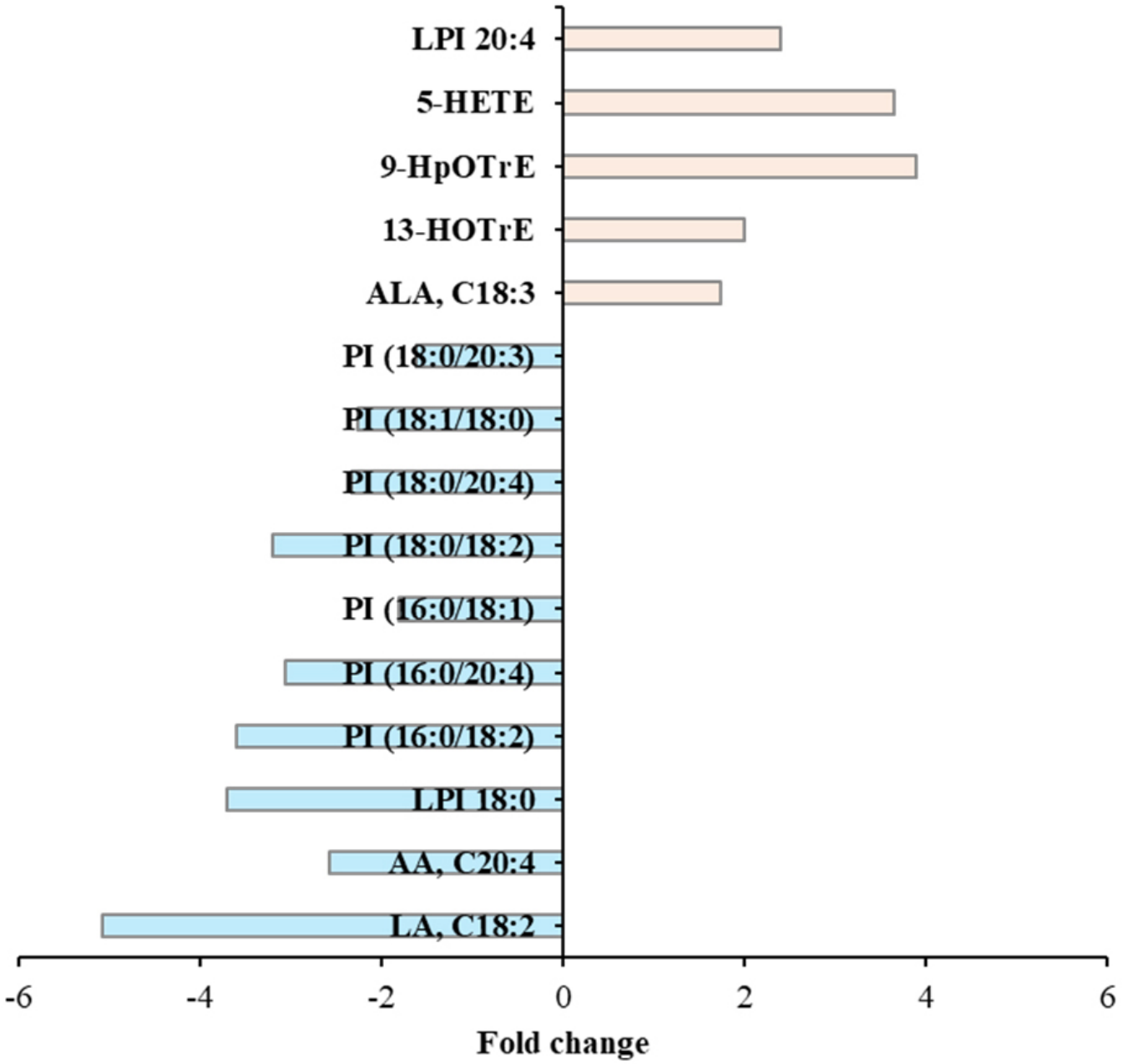


Figure 5

The fold changes in the concentrations of oxidized fatty acids, ALA, AA, LA, and PIs in the erythrocytes of COVID-19 patients versus healthy volunteers, n = 30.

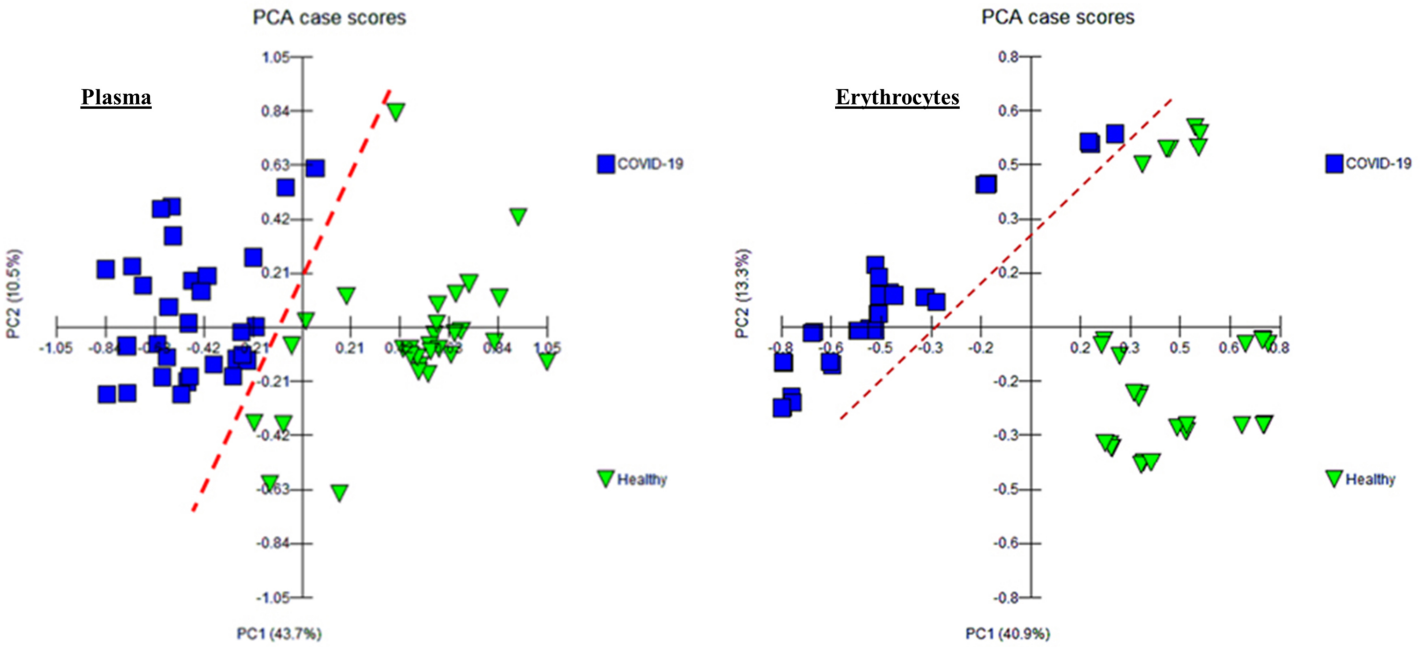


Figure 6

Principal component analysis (PCA), PC1 vs. PC2. The score plot shows separation between COVID-19 cases (blue) and healthy volunteers (green) based on the abundance of phospholipids significantly dysregulated in plasma and erythrocytes ($p<0.05$), n = 30.

Supplementary Files

This is a list of supplementary files associated with this preprint. Click to download.

- SUPPLEMENTARY.docx
- GAbstract.jpg